Available online at www.sciencedirect.com
ScienceDirect
Geochimica et Cosmochimica Acta 73 (2009) 7203–7225
Geochimica et Cosmochimica Acta
www.elsevier.com/locate/gca

Isotopic fractionations associated with phosphoric acid digestion of carbonate minerals: Insights from first-principles theoretical modeling and clumped isotope measurements

Weifu Guo [a,*], Jed L. Mosenfelder [a], William A. Goddard III [b], John M. Eiler [a]

[a] *Division of Geological and Planetary Sciences, California Institute of Technology, Pasadena, CA 91125, USA*
[b] *Materials and Process Simulation Center, California Institute of Technology, Pasadena, CA 91125, USA*

Received 28 July 2008; accepted in revised form 27 May 2009; available online 23 June 2009

Abstract

Phosphoric acid digestion has been used for oxygen- and carbon-isotope analysis of carbonate minerals since 1950, and was recently established as a method for carbonate 'clumped isotope' analysis. The CO_2 recovered from this reaction has an oxygen isotope composition substantially different from reactant carbonate, by an amount that varies with temperature of reaction and carbonate chemistry. Here, we present a theoretical model of the kinetic isotope effects associated with phosphoric acid digestion of carbonates, based on structural arguments that the key step in the reaction is disproportionation of H_2CO_3 reaction intermediary. We test that model against previous experimental constraints on the magnitudes and temperature dependences of these oxygen isotope fractionations, and against new experimental determinations of the fractionation of ^{13}C–^{18}O-containing isotopologues ('clumped' isotopic species). Our model predicts that the isotope fractionations associated with phosphoric acid digestion of carbonates at 25 °C are 10.72‰, 0.220‰, 0.137‰, 0.593‰ for, respectively, $^{18}O/^{16}O$ ratios ($1000\ln\alpha^*$) and three indices that measure proportions of multiply-substituted isotopologues ($\Delta^*_{47}, \Delta^*_{48}, \Delta^*_{49}$). We also predict that oxygen isotope fractionations follow the mass dependence exponent, λ of 0.5281 (where $\alpha_{17_O} = \alpha'_{18_O}$). These predictions compare favorably to independent experimental constraints for phosphoric acid digestion of calcite, including our new data for fractionations of ^{13}C–^{18}O bonds (the measured change in $\Delta_{47} = 0.23‰$) during phosphoric acid digestion of calcite at 25 °C.

We have also attempted to evaluate the effect of carbonate cation compositions on phosphoric acid digestion fractionations using cluster models in which disproportionating H_2CO_3 interacts with adjacent cations. These models underestimate the magnitude of isotope fractionations and so must be regarded as unsucsessful, but do reproduce the general trend of variations and temperature dependences of oxygen isotope acid digestion fractionations among different carbonate minerals. We suggest these results present a useful starting point for future, more sophisticated models of the reacting carbonate/acid interface. Examinations of these theoretical predictions and available experimental data suggest cation radius is the most important factor governing the variations of isotope fractionation among different carbonate minerals. We predict a negative correlation between acid digestion fractionation of oxygen isotopes and of ^{13}C–^{18}O doubly-substituted isotopologues, and use this relationship to estimate the acid digestion fractionation of Δ^*_{47} for different carbonate minerals. Combined with previous theoretical evaluations of ^{13}C–^{18}O clumping effects in carbonate minerals, this enables us to predict the temperature calibration relationship for different carbonate clumped isotope thermometers (witherite, calcite, aragonite, dolomite and magnesite), and to compare these predictions with available experimental determinations. The success of our models in capturing several of the features of isotope fractionation during acid digestion supports our hypothesis that phosphoric acid digestion of carbonate minerals involves disproportionation of transition state structures containing H_2CO_3.

* Corresponding author. Present address: Geophysical Laboratory, Carnegie Institution of Washington, Washington DC 20015, USA. Tel.: +1 202 478 8993; fax: +1 202 478 8901.
E-mail address: wfguo@ciw.edu (W. Guo).

0016-7037/$ - see front matter © 2009 Elsevier Ltd. All rights reserved.
doi:10.1016/j.gca.2009.05.071

1. INTRODUCTION

Analysis of the stable isotope compositions of carbonate minerals is among the most common and useful measurements in isotope geochemistry. For example, much of paleoclimatology is based on the carbonate–water oxygen isotope thermometry (Urey, 1947) and most records of the global carbon cycle through time depend on measuring the carbon isotope compositions of sedimentary carbonates (Des Marais, 1997). More recently, Ghosh et al. (2006) and Schauble et al. (2006) developed a carbonate 'clumped isotope' thermometer based on the ordering of ^{13}C and ^{18}O into bonds with each other within the carbonate mineral lattice.

These stable isotope measurements of carbonates are generally performed indirectly by reacting the sample carbonate with anhydrous phosphoric acid and then analyzing the product CO_2 on a gas source isotope ratio mass spectrometer (McCrea, 1950). This method is relatively straightforward to perform, is applicable to a wide range of sample sizes, has been automated in several different ways, and is exceptionally precise. These features make this approach preferable to alternative methods for most applications (e.g., fluorination, Sharma and Clayton, 1965; secondary ion mass spectrometry, Rollion-Bard et al., 2007; laser ablation, Sharp and Cerling, 1996). However because only two out of three oxygen atoms in carbonate are released as CO_2 during phosphoric acid digestion, this method involves a kinetic oxygen isotope fractionation; i.e., product CO_2 is ~10‰ higher in $\delta^{18}O$ than reactant carbonate (Gilg et al., 2003 and reference therein). The exact magnitude of this kinetic fractionation varies with acid digestion temperature and appears to differ among carbonate minerals (Sharma and Clayton, 1965; Kim and O'Neil, 1997; Gilg et al., 2003). Similarly, preliminary evidence suggests that values of Δ_{47} (a measure of the abundance anomaly of ^{13}C–^{18}O bonds in CO_2; defined as $\Delta_{47} = \left(\frac{R^{47}_{\text{actual}}}{R^{47}_{\text{stochastic}}} - 1\right) \times 1000$; Eiler and Schauble, 2004) are enriched in CO_2 produced by acid digestion of calcite and aragonite relative to values one expects in the absence of any associated fractionation (Ghosh et al., 2006). These analytical fractionations must be corrected for in any study of the oxygen isotope or 'clumped isotope' compositions of carbonate minerals.

The oxygen isotope fractionations associated with phosphoric acid digestion of different carbonate minerals have been experimentally studied over a range of temperatures (Sharma and Clayton, 1965; Sharma and Sharma, 1969a,b; Rosenbaum and Sheppard, 1986; Swart et al., 1991; Bottcher, 1996; Kim and O'Neil, 1997; Gilg et al., 2003; Kim et al., 2007). However, there are significant discrepancies among acid digestion fractionations of oxygen isotopes determined in different studies (Kim et al., 2007 and reference therein). For example, reported acid digestion fractionations at 25 °C range from 10.10‰ (Das Sharma et al., 2002) to 10.52‰ (Land, 1980) for calcite, and from 10.29‰ (Sharma and Clayton, 1965) to 11.01‰ (Kim and O'Neil, 1997) for aragonite. Even within a single study, the measured acid digestion fractionation factors for the same type of carbonate minerals can vary among different samples of the same phase (as much as ~2‰ for octavite, ~0.6‰ for witherite and ~0.5‰ for calcite at 25 °C; Kim and O'Neil, 1997). More generally, our understanding of this phenomenon is entirely empirical, and thus provides little basis for extrapolation to new materials or conditions of acid digestion.

Our understanding of acid digestion fractionations is particularly poor in relation to the carbonate 'clumped isotope' thermometer (Ghosh et al., 2006). It has been shown that the abundance anomaly of ^{13}C–^{18}O bonds in CO_2 produced by acid digestion of carbonate differs from that in reactant carbonate (Ghosh et al., 2006), but the exact magnitude of this fractionation was poorly constrained and its variation among different carbonate minerals is unexplored. These gaps in our understanding limit the use of the carbonate clumped isotope thermometer for minerals other than calcite and aragonite, e.g., dolomite or magnesite. Because these carbonates are difficult to synthesize in isotopic equilibrium (especially at ambient temperatures), theoretical understandings of both ^{13}C–^{18}O clumping within minerals (Schauble et al., 2006) and clumped isotope fractionations during acid digestion are important guides to interpreting observations on natural samples.

To the best of our knowledge, no detailed theoretical model has been proposed to explain the isotope fractionations that accompany phosphoric acid digestion of carbonate minerals. Sharma and Sharma (1969b) determined the oxygen isotope acid digestion fractionation factors for several different carbonate minerals, and explained them as a result of two factors: a temperature-dependent factor and a temperature-independent factor. Sharma and Sharma (1969b) further suggested the temperature-independent factor varies as a function of the atomic mass of the cations in carbonate minerals, and can be explained by their proposed structure for the transition state through which the acid digestion reaction proceeds (Fig. 1a). However, Sharma and Sharma's model does not quantitatively describe the temperature-dependent factor, and subsequent experimental results (Bottcher, 1996; Gilg et al., 2003) are inconsistent with their model.

In this study, we present a quantitative model of the phosphoric acid digestion reaction based on transition sate theory and statistical thermodynamics. We use this model to predict isotopic fractionations among all isotopologues (including multiply substituted isotopologues) of reactant carbonate ions, and thus the isotopic composition (including abundances of multiply-substituted isotopologues) of CO_2 produced by phosphoric acid digestion of carbonate minerals. Finally, we test the accuracy of our model by comparison with previous data documenting the oxygen isotope fractionation associated with this reaction, and with new data we have generated documenting the fractionation of ^{13}C–^{18}O bearing isotopologues during acid digestion (which controls the Δ_{47} value of product CO_2). We observe quantitative agreements between our model predictions and available experimental data on the magnitude and temperature dependence of isotope fractionations associated with phosphoric acid digestion for calcite. We then modify this model to explore the effect of cation content on the acid digestion fractionation; this effort fails to yield an accurate match to experimental data—

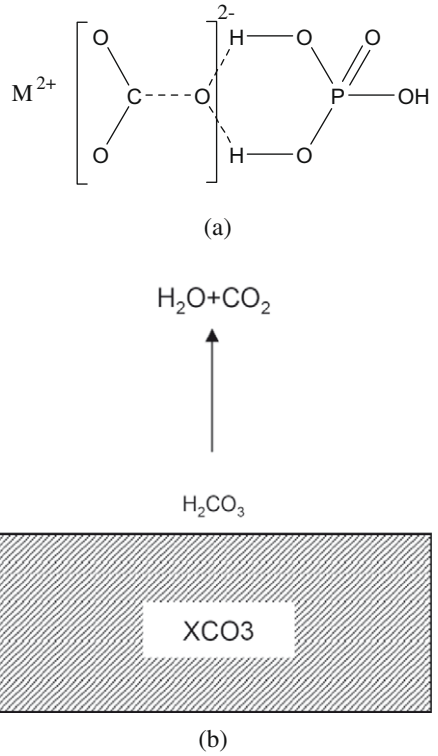

Fig. 1. Reaction mechanisms during phosphoric acid digestion of carbonate minerals, proposed by (a) Sharma and Sharma (1969b), and (b) this study. See Section 2.2.1 for details.

presumably because our guess regarding the structure of the carbonate-acid interface is imperfect. Nevertheless, it yields a trend of variations of oxygen isotope fractionations with cation identity that resembles experimental data, and thus the approach may be a fruitful starting point for future, more sophisticated models.

This study provides a framework for understanding isotope fractionations accompanying phosphoric acid digestion of carbonate minerals, and applying them to conditions or materials that are not yet understood through experimental work. Furthermore, this study demonstrates a technique of first-principles modeling of kinetic isotope effects associated with irreversible reactions and illustrates the utility of this technique by application to one of the more extensively studied inorganic reactions in stable isotope geochemistry, taking advantage of new constraints provided by clumped isotope measurements. This approach therefore serves as a model for future work of similar but less well known kinetically-controlled fractionations.

2. THEORETICAL AND COMPUTATIONAL METHODS

2.1. Transition state theory of reaction rates

Transition state theory is long established as a tool for studying chemical kinetics (Eyring, 1935a,b) and has been used previously to understand irreversible reactions in geoscience problems (Lasaga, 1998; Felipe et al., 2001). Classical transition state theory is based on two key assumptions (Felipe et al., 2001): (1) instead of transforming directly into products, reactants in a chemical reaction first proceed through an unstable chemical state called the "transition state", which has a higher chemical potential energy than reactants or products; (2) the transition state may only form from the reactants (i.e., the conversion of the transition state to products is irreversible), and any transition state that proceeds in the reaction coordinate past its potential energy maximum must eventually form products. This second assumption is also called the "non-recrossing rule". For example, transition state theory would describe $A + B \rightarrow C + D$ as proceeding through two steps: reversible transformation of reactants A and B into a transition state, $M^\dagger$, after which $M^\dagger$ transforms irreversibly into products C and D (i.e. $A + B \overset{1}{\rightleftarrows} M^\dagger \overset{2}{\rightarrow} C + D$). Therefore, the rate of the overall reaction (i.e. the production rate of C and D), R, equals the decomposition rate of the transition state, $M^\dagger$ and can be described through the relation:

$$R = \frac{[M^\dagger]}{\tau} = |v_L^\dagger|[M^\dagger] \quad (1)$$

where $[M^\dagger]$ is the concentration of transition state $M^\dagger$, τ is the average lifetime of transition state $M^\dagger$ and $v_L^\dagger$ is the 'decomposition frequency' (defined as the reciprocal of the average life time) of $M^\dagger$ (Melander and Saunders, 1987; Felipe et al., 2001). The concentration of the transition state, $[M^\dagger]$, can be estimated by assuming that the reversible reaction, $A + B \overset{1}{\rightleftarrows} M^\dagger$, is at equilibrium (Melander and Saunders, 1987):

$$[M^\dagger] = K[A][B] \quad (2)$$

where [A] and [B] are the concentrations of reactant A and B respectively, and K is the equilibrium constant for reaction 1 and is evaluated using statistical thermodynamics (Urey, 1947):

$$K = \frac{Q^\dagger}{Q_A \times Q_B} = \frac{s_A \times s_B}{s^\dagger} \frac{\prod_i^{3N^\dagger-7}\left(u_i^\dagger \times \frac{1}{e^{\frac{1}{2}u_i^\dagger}} \times \frac{1}{1-e^{-u_i^\dagger}}\right)}{\prod_{j_A}^{3N_A-6}\left(u_{j_A} \times \frac{1}{e^{\frac{1}{2}u_{j_A}}} \times \frac{1}{1-e^{-u_{j_A}}}\right) \times \prod_{j_B}^{3N_B-6}\left(u_{j_B} \times \frac{1}{e^{\frac{1}{2}u_{j_B}}} \times \frac{1}{1-e^{-u_{j_B}}}\right)}$$

$$u_i^\dagger = \frac{hc\varpi_i^\dagger}{kT}, \quad u_{j_A} = \frac{hc\varpi_{j_A}}{kT}, \quad u_{j_B} = \frac{hc\varpi_{j_B}}{kT} \quad (3)$$

where $Q^\dagger$, Q_A, Q_B are the partition functions of transition state $M^\dagger$ and reactants, A and B, respectively; $\varpi_i^\dagger, \varpi_{j_A}, \varpi_{j_B}$ are the vibration frequencies, in wave numbers, for the transition state $M^\dagger$and reactants, A and B, respectively (one such term is required for each mode of vibration of each species); $s^\dagger$, s_A, s_B are the symmetry numbers for transition state $M^\dagger$ and reactants A and B, respectively; $N^\dagger$, N_A, N_B are the numbers of atoms within transition state $M^\dagger$ and reactants, A and B, respectively; h is Plank's constant; c is the velocity of light; k is the Boltzmann constant; and T is the reaction temperature in Kelvin.

When one is interested in kinetic isotope effects, as in this study, *relative* reaction rates (i.e., the ratios of reaction rates of different isotopologues) are of greatest importance:

$$\frac{R_{(1)}}{R_{(2)}} = \frac{|v_L^{\dagger}|_{(1)}[M^{\dagger}]_{(1)}}{|v_L^{\dagger}|_{(2)}[M^{\dagger}]_{(2)}} \quad (4)$$

where subscript (1) and (2) denote different isotopologues of the transition state.

2.2. Application of transition state theory to phosphoric acid digestion of carbonate minerals

2.2.1. Proposed reaction mechanism and transition state structure during phosphoric acid digestion of carbonate minerals

In order to calculate the partition function of the transition state associated with phosphoric acid digestion of carbonates, we must first determine or assume the transition state structure. This is commonly done by initially guessing the structure of transition state and then refining on that guess using ab inito calculations (Felipe et al., 2001).

Little is known about the exact reaction mechanism and transition state structure during the phosphoric acid digestion of carbonate minerals. Although the transition state structure suggested by Sharma and Sharma (1969b) is intuitively appealing (Fig. 1a), there is no evidence to date that supports it. Instead, recent spectroscopic studies of calcium carbonate undergoing reactions with anhydrous acidic gases (e.g., HNO_3, SO_2, HCOOH and CH_3COOH) identified absorbed H_2CO_3 on the carbonate surface and suggested carbonic acid as the important intermediate species during these reactions (Al-Hosney and Grassian, 2004; Al-Hosney and Grassian, 2005). Though carbonic acid decomposes rapidly in aqueous solution, it is kinetically stable in the absence of water (Hage et al., 1998; Loerting et al., 2000 and reference therein). We suggest that these experiments are analogous to the local environment at the surface of a carbonate mineral during reaction with anhydrous phosphoric acid (i.e., the 105% concentrated phosphoric acid used in stable isotope analyses of carbonates; Coplen et al., 1983). We therefore propose that H_2CO_3 is also an intermediate during phosphoric acid digestion of carbonate minerals, i.e. this reaction, $XCO_3 + H_3PO_4 \rightarrow XHPO_4 + CO_2 + H_2O$, proceeds through two steps (Fig. 1b):

$$XCO_3 + H_3PO_4 \xrightarrow{1} XHPO_4 + H_2CO_3$$

$$H_2CO_3 \xrightarrow{2} CO_2 + H_2O$$

where X is a cation, such as Ca, contained in the carbonate mineral.

We infer that the first of these two reaction steps should be associated with little or no net isotopic fractionation (including fractionations of multiply-substituted isotopologues), for two reasons: (1) in practice, phosphoric acid digestion is always driven to completion before collecting and analyzing product CO_2. Because CO_3^{2-} ionic units in the reactant carbonate are quantitatively converted into H_2CO_3 during step 1, it is not possible to express a net isotopic fractionation of C or O isotopes during that step, even if that reaction has some intrinsic kinetic isotope effect. And, (2) any kinetic isotope effect that might accompany step 1 could only be expressed if the site at which the reaction occurs (i.e., a mineral surface) can undergo isotopic exchange with the unreacted mineral interior, which we consider unlikely at the low temperatures and anhydrous conditions of phosphoric acid digestion. That is, we infer that step 1 is analogous to sublimation of ice, which generally fails to express a vapor pressure isotope effect because the reaction effectively 'peels' away layers of the solid without leaving an isotopically modified residue. Similarly, we assume no oxygen isotope exchange between the carbonic acid and the surrounding anhydrous phosphoric acids and among different carbonic acid isotopologues during the phosphoric acid digestion. In order for such exchange to occur, C–O bonds in the carbonic acid would have to break and reform. We regard this as unlikely given the kinetic stability of carbonic acid under anhydrous environments (Loerting et al., 2000; Hage et al., 1998 and reference therein). For these reasons, we focus on step 2—the dissociation of carbonic acid.

No prior studies exist on the exact bonding environment of intermediate H_2CO_3 during phosphoric acid digestion of carbonate minerals. In the following model, we describe the intermediate H_2CO_3 as free isolated molecules, and take a previously determined transition state structure for gas phase carbonic acid decomposition (Loerting et al., 2000) as our 'initial guess' (Fig. 2b). We then optimize that structure through further ab initio calculations. It is reasonable to suspect that the presence of unreacted carbonate surface and surrounding H_3PO_4 might also affect the decomposition of the intermediate H_2CO_3 during phosphoric acid digestion of carbonate minerals. For example, intermediate H_2CO_3 might exist as absorbed molecules and dissociate on the unreacted carbonate surface. These interactions would then introduce second order effects on the kinetic isotope effects associated with phosphoric acid digestion. We attempt to evaluate the interactions between H_2CO_3 and un-reacted mineral surface through a 'cluster model' in Section 2.2.3. We did not consider potential interactions between H_2CO_3 and surrounding H_3PO_4, which requires more sophisticated model and computational capacity beyond the scope of this study.

2.2.2. Fractionation of CO_3^{2-} isotopologues during dissociation of carbonic acid

Carbonic acid, H_2CO_3, has 20 naturally occurring isotopologues, not counting those containing D or ^{14}C, which can dissociate to produce 12 different isotopologues of product CO_2 (Table 1). Furthermore, many of the isotopologues of H_2CO_3 have more than one isotopomer because the various O sites are not structurally equivalent to one another (see Fig. 2). To distinguish the isotopologues and isotopomers in our following discussion, formula expressions for isotopomers are underlined, with their oxygen atoms expressed in the order of position 2, 3 and 4 in Fig. 2 (note, oxygen atoms at position 4 are the ones to be abstracted during phosphoric acid digestion). For example, $\underline{H_2\,C^{18}O^{16}O^{16}O}$, $\underline{H_2C^{16}O^{18}O^{16}O}$ and $\underline{H_2\,C^{16}O^{16}O^{18}O}$ denote the three isotopomers of the $H_2C^{18}O^{16}O_2$ isotopologue, with ^{18}O occupying the oxygen position 2, 3 and 4, respectively, (Fig. 2d–f). Similarly, the formula expressions for transition state structures in the following

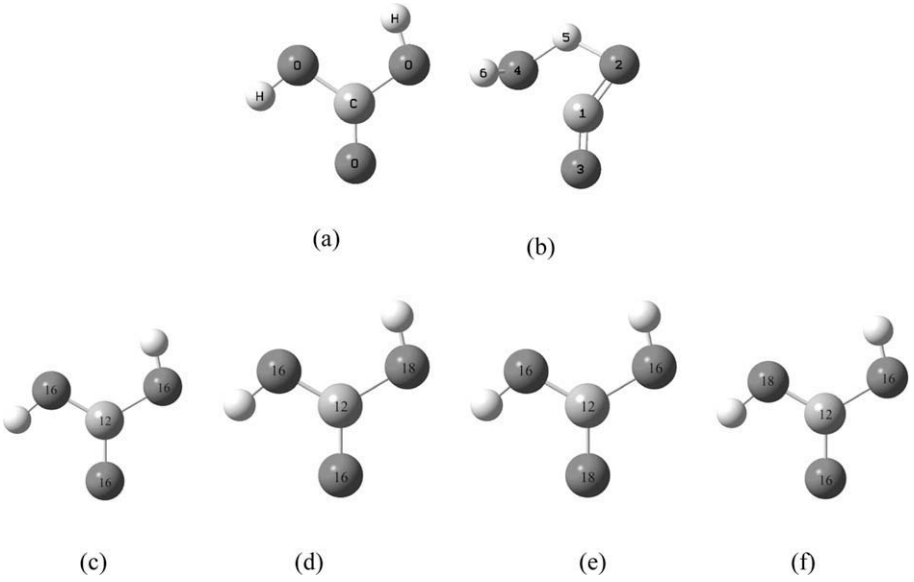

Fig. 2. Optimized transition state structures during phosphoric acid digestion of carbonate minerals (H_2CO_3 dissociation model): (a) an optimized stable structure of carbonic acid, shown for comparison; (b) the optimized transition state structure employed in the ab initio calculations of this study. Numbers refer to atomic positions within the structure. Oxygen atom 4 is the one that is abstracted from the reactant carbonate ion during acid digestion (i.e., oxygen atoms 2 and 3 remain bound to carbon atom 1); (c) the only carbonic acid isotopomer ($\underline{H_2{}^{12}C^{16}O\ {}^{16}O^{16}O}$) during the phosphoric acid digestion of $^{12}C^{16}O_3{}^{2-}$. Numbers refer to the isotopic mass, in AMU, of the atom; (d–f) three possible carbonic acid isotopomers ($\underline{H_2{}^{12}C^{18}O^{16}O^{16}O}$, $\underline{H_2{}^{12}C^{16}O^{18}O^{16}O}$ and $\underline{H_2{}^{12}C^{16}O^{16}O^{18}O}$, respectively) during the phosphoric acid digestion of $^{12}C^{18}O^{16}O_2^{2-}$. Numbers again refer to isotopic mass of the atom.

discussions are superscripted with "†" signs, in order to distinguish them from those for stable molecules.

Isotopic fractionations during the dissociation of carbonic acid can arise for two reasons: (1) the various isotopologues of carbonic acid differ from one another in their rates of dissociation (e.g., the rate of dissociation of $H_2{}^{12}C^{16}O_3$ is faster than the weighted average dissociation rate of the three isotopomers of $H_2{}^{12}C^{18}O^{16}O_2$; Fig. 2c–f); and (2) when an isotopologue has more than one isotopomer (e.g., Fig. 2), the relative rates of dissociation of those isotopomers differ from one another. However, since phosphoric acid digestion is always driven to completion before collecting and analyzing product CO_2 (i.e., all isotopologues of carbonic acid eventually decompose) and we assume there is no isotope exchange between different H_2CO_3 isotopologues, the first type of isotope effects will not be expressed in the final isotopic composition of product CO_2 (though they might influence the temporal evolution of the isotopic composition of product CO_2). Only the second type of isotope effects contributes to the fact that final product CO_2 is expected to be higher in $^{18}O/^{16}O$ ratio than the reactant H_2CO_3. For example, differences between the rates of dissociation of the three isotopomers of $H_2{}^{12}C^{18}O^{16}O_2$ promote production of $^{12}C^{18}O^{16}O$ relative to $^{12}C^{16}O_2$ (i.e., those isotopomers that must break a ^{12}C–^{16}O bond in order to dissociate [Fig. 2d and e] do so more quickly than those isotopomers that must break a ^{12}C–^{18}O bond [Fig. 2f]).

We calculate the proportions of CO_2 isotopologues produced by dissociation of each H_2CO_3 isotopologue based on a formulation that is exemplified as follows for the case of $H_2{}^{12}C^{18}O^{16}O_2$. This isotopologue of carbonic acid consists of three isotopomers, which dissociate to form two isotopologues of CO_2, $^{12}C^{16}O_2$ and $^{12}C^{18}O^{16}O$ (Fig. 2). The relative abundance of each of these products is calculated through the equations:

$$n_{^{12}C^{16}O_2-H_2{}^{12}C^{18}O^{16}O_2} = \frac{R_{^{12}C^{16}O_2-\underline{H_2{}^{12}C^{16}O^{16}O^{18}O}}}{R_{^{12}C^{18}O^{16}O-\underline{H_2{}^{12}C^{18}O^{16}O^{16}O}} + R_{^{12}C^{18}O^{16}O-\underline{H_2{}^{12}C^{16}O^{18}O^{16}O}} + R_{^{12}C^{16}O_2-\underline{H_2{}^{12}C^{16}O^{16}O^{18}O}}} \times n_{H_2{}^{12}C^{18}O^{16}O_2} \quad (5)$$

$$n_{^{12}C^{18}O^{16}O-H_2{}^{12}C^{18}O^{16}O_2} = \frac{R_{^{12}C^{18}O^{16}O-\underline{H_2{}^{12}C^{18}O^{16}O^{16}O}} + R_{^{12}C^{18}O^{16}O-\underline{H_2{}^{12}C^{16}O^{18}O^{16}O}}}{R_{^{12}C^{18}O^{16}O-\underline{H_2{}^{12}C^{18}O^{16}O^{16}O}} + R_{^{12}C^{18}O^{16}O-\underline{H_2{}^{12}C^{16}O^{18}O^{16}O}} + R_{^{12}C^{16}O_2-\underline{H_2{}^{12}C^{16}O^{16}O^{18}O}}} \times n_{H_2{}^{12}C^{18}O^{16}O_2} \quad (6)$$

where $n_{^{12}C^{16}O_2-H_2{}^{12}C^{18}O^{16}O_2}$ and $n_{^{12}C^{18}O^{16}O-H_2{}^{12}C^{18}O^{16}O_2}$ denote the total numbers of molecules of $^{12}C^{16}O_2$ and $^{12}C^{18}O^{16}O$ produced from dissociation of $H_2{}^{12}C^{18}O^{16}O_2$; $n_{H_2{}^{12}C^{18}O^{16}O_2}$ is the number of molecules of reactant $H_2{}^{12}C^{18}O^{16}O_2$, which we take to equal the abundance of $X^{12}C^{18}O^{16}O_2$ in the carbonate undergoing phosphoric acid digestion; i.e., we ignore any isotopic discrimination associated with step 1 of the overall reaction and any isotope exchange between different H_2CO_3 isotopologues, as defined in Section 2.2.1. $R_{^{12}C^{18}O^{16}O-\underline{H_2{}^{12}C^{18}O^{16}O^{16}O}}$, $R_{^{12}C^{18}O^{16}O-\underline{H_2{}^{12}C^{16}O^{18}O^{16}O}}$ and $R_{^{12}C^{16}O_2-\underline{H_2{}^{12}C^{16}O^{16}O^{18}O}}$ denote the dissociation rates of the three isotopomers of $H_2{}^{12}C^{18}O^{16}O_2$ (Fig. 2). These R values are calculated based on statistical thermodynamic principles, as described in Section 2.1 and exemplified below:

$$R_{^{12}C^{18}O^{16}O-\underline{H_2{}^{18}O^{16}O^{16}O}} = |\nu_L^{\dagger}|_{\underline{H_2{}^{12}C^{18}O^{16}O^{16}O^{\dagger}}} \times \frac{Q^{\dagger}_{\underline{H_2{}^{12}C^{18}O^{16}O^{16}O^{\dagger}}}}{Q_{\underline{H_2{}^{12}C^{18}O^{16}O^{16}O}}} \times [\underline{H_2{}^{12}C^{18}O^{16}O^{16}O}] \quad (7)$$

Table 1
Evolution of different CO_3^{2-} isotopologues during phosphoric acid digestion of carbonate minerals.

Isotopologue of CO_3^{2-} Reactant	Mass[a]	Abundance of CO_3^{2-} Isotopologues[b]	Isotopomer of H_2CO_3Intermediate[c]	Isotopologue of CO_2Product	Mass[a]	Fraction[d]
$^{12}C^{16}O^{16}O^{16}O^{2-}$	60	0.981845503	$H_2{}^{12}C^{16}O^{16}O^{16}O$	$^{12}C^{16}O^{16}O$	44	1
$^{13}C^{16}O^{16}O^{16}O^{2-}$	61	0.011033194	$H_2{}^{13}C\ {}^{16}O^{16}O^{16}O$	$^{13}C^{16}O^{16}O$	45	1
$^{12}C^{17}O^{16}O^{16}O^{2-}$	61	0.000373003	$H_2{}^{12}C^{17}O\ {}^{16}O^{16}O$	$^{12}C^{17}O^{16}O$	45	0.3345939
			$H_2{}^{12}C^{16}O\ {}^{17}O^{16}O$	$^{12}C^{17}O^{16}O$	45	0.3358595
			$H_2{}^{12}C^{16}O\ {}^{16}O^{17}O$	$^{12}C^{16}O^{16}O$	44	0.3295466
$^{12}C^{18}O^{16}O^{16}O^{2-}$	62	0.001968797	$H_2{}^{12}C\ {}^{18}O^{16}O^{16}O$	$^{12}C^{18}O^{16}O$	46	0.3357121
			$H_2{}^{12}C^{16}O\ {}^{18}O^{16}O$	$^{12}C^{18}O\ {}^{16}O$	46	0.3381400
			$H_2{}^{12}C^{16}O\ {}^{16}O^{18}O$	$^{12}C^{16}O^{16}O$	44	0.3261479
$^{13}C^{17}O^{16}O^{16}O^{2-}$	62	4.19151E−06	$H_2{}^{13}C^{17}O\ {}^{16}O^{16}O$	$^{13}C^{17}O^{16}O$	46	0.3345930
			$H_2{}^{13}C^{16}O\ {}^{17}O^{16}O$	$^{13}C\ {}^{17}O^{16}O$	46	0.3359415
			$H_2{}^{13}C\ {}^{16}O^{16}O^{17}O$	$^{13}C^{16}O^{16}O$	45	0.3359415
$^{12}C^{17}O^{17}O^{16}O^{2-}$	62	1.41704E−07	$H_2{}^{12}C\ {}^{17}O^{17}O\ {}^{16}O$	$^{12}C^{17}O^{17}O$	46	0.3371440
			$H_2{}^{12}C\ {}^{17}O^{16}O^{17}O$	$^{12}C^{17}O^{16}O$	45	0.3308090
			$H_2{}^{12}C^{16}O\ {}^{17}O^{17}O$	$^{12}C^{17}O^{16}O$	45	0.3320470
$^{13}C^{18}O^{16}O^{16}O^{2-}$	63	2.21238E−05	$H_2{}^{13}C\ {}^{18}O^{16}O^{16}O$	$^{13}C^{18}O^{16}O$	47	0.3357094
			$H_2{}^{13}C^{16}O\ {}^{18}O^{16}O$	$^{13}C\ {}^{18}O^{16}O$	47	0.3382969
			$H_2{}^{13}C\ {}^{16}O^{16}O\ {}^{18}O$	$^{13}C^{16}O^{16}O$	45	0.3259937
$^{12}C^{18}O^{17}O^{16}O^{2-}$	63	7.47946E−07	$H_2{}^{12}C^{18}O\ {}^{17}O^{16}O$	$^{12}C\ {}^{18}O^{17}O$	47	0.1691418
			$H_2{}^{12}C^{18}O\ {}^{16}O^{17}O$	$^{12}C^{18}\ O^{16}O$	46	0.1659645
			$H_2{}^{12}C^{17}O\ {}^{18}O^{16}O$	$^{12}C^{17}\ O^{18}O$	47	0.1697232
			$H_2{}^{12}C^{17}O\ {}^{16}O^{18}O$	$^{12}C^{17}\ O^{16}O$	45	0.1637057
			$H_2{}^{12}C^{16}O\ {}^{18}O^{17}O$	$^{12}C^{18}\ O^{16}O$	46	0.1671522
			$H_2{}^{12}C^{16}O\ {}^{17}O^{18}O$	$^{12}C^{17}\ O^{16}O$	47	0.1643126
$^{13}C^{17}O^{17}O^{16}O^{2-}$	63	1.59235E−09	$H_2{}^{13}C^{17}O\ {}^{17}O^{16}O$	$^{13}C^{17}O\ {}^{17}O$	47	0.3372255
			$H_2{}^{13}C^{17}O\ {}^{16}O^{17}O$	$^{13}C^{17}\ O^{16}O$	46	0.3307273
			$H_2{}^{13}C^{16}O\ {}^{17}O^{17}O$	$^{13}C^{17}\ O^{16}O$	46	0.3320472
$^{12}C^{17}O^{17}O^{17}O^{2-}$	63	5.38333E− 11	$H_2{}^{12}C^{17}O\ {}^{17}O^{17}O$	$^{12}C^{17}\ O^{17}O$	46	1
$^{12}C^{18}O^{18}O^{16}O^{2-}$	64	3.94783E− 06	$H_2{}^{12}C^{18}O\ {}^{18}O^{16}O$	$^{12}C^{18}\ O^{18}O$	48	0.3406058
			$H_2{}^{12}C^{18}O\ {}^{16}O^{18}O$	$^{12}C^{18}\ O^{16}O$	46	0.3285328
			$H_2{}^{12}C^{16}O\ {}^{18}O^{18}O$	$^{12}C^{18}\ O^{16}O$	46	0.3308614
$^{13}C^{18}O^{17}O^{16}O^{2-}$	64	8.40482E− 09	$H_2{}^{13}C^{18}O\ {}^{17}O^{16}O$	$^{13}C^{18}\ O^{17}O$	48	0.1691819
			$H_2{}^{13}C^{18}O\ {}^{16}O^{17}O$	$^{13}C^{18}\ O^{16}O$	47	0.1659230
			$H_2{}^{13}C^{17}O\ {}^{18}O^{16}O$	$^{13}C^{18}\ O^{17}O$	48	0.1698016
			$H_2{}^{13}C^{17}O\ {}^{16}O^{18}O$	$^{13}C^{17}\ O^{16}O$	46	0.1636285
			$H_2{}^{13}C^{16}O\ {}^{18}O^{17}O$	$^{13}C^{18}\ O^{16}O$	47	0.1671893
			$H_2{}^{13}C^{16}O\ {}^{17}O^{18}O$	$^{13}C^{17}\ O^{16}O$	46	0.1642757
$^{12}C^{18}O^{17}O^{17}O^{2-}$	64	2.84145E−10	$H_2{}^{12}C^{18}O\ {}^{17}O^{17}O$	$^{12}C^{18}O\ {}^{17}O$	47	0.3344749
			$H_2{}^{12}C^{17}O\ {}^{18}O^{17}O$	$^{12}C^{18}\ O^{17}O$	47	0.3356125
			$H_2{}^{12}C^{17}O\ {}^{17}O^{18}O$	$^{12}C^{17}\ O^{17}O$	46	0.3299126
$^{13}C^{17}O^{17}O^{17}O^{2-}$	64	6.04936E− 13	$H_2{}^{13}C^{17}O\ {}^{17}O^{17}O$	$^{13}C^{17}\ O^{17}O$	47	1
$^{13}C^{18}O^{18}O^{16}O^{2-}$	65	4.43626E− 08	$H_2{}^{13}C^{18}O\ {}^{18}O^{16}O$	$^{13}C^{18}\ O^{18}O$	49	0.3407615
			$H_2{}^{13}C^{18}O\ {}^{16}O^{18}O$	$^{13}C^{18}\ O^{16}O$	47	0.3283773
			$H_2{}^{13}C^{16}O\ {}^{18}O^{18}O$	$^{13}C^{18}\ O^{16}O$	47	0.3308612
$^{12}C^{18}O^{18}O^{17}O^{2-}$	65	1.49978E− 09	$H_2{}^{12}C^{18}O\ {}^{18}O^{17}O$	$^{12}C^{18}\ O^{18}O$	48	0.3367737
			$H_2{}^{12}C^{18}O\ {}^{17}O^{18}O$	$^{12}C^{18}\ O^{17}O$	47	0.3310555
			$H_2{}^{12}C^{17}O\ {}^{18}O^{18}O$	$^{12}C^{18}\ O^{17}O$	47	0.3321708
$^{13}C^{18}O^{17}O^{17}O^{2-}$	65	3.19299E− 12	$H_2{}^{13}C^{18}O\ {}^{17}O^{17}O$	$^{13}C^{18}\ O^{17}O$	48	0.3344739
			$H_2{}^{13}C^{17}O\ {}^{18}O^{17}O$	$^{13}C^{18}\ O^{17}O$	48	0.3356870
			$H_2{}^{13}C^{17}O\ {}^{17}O^{18}O$	$^{13}C^{17}\ O^{17}O$	47	0.3298391
$^{12}C^{18}O^{18}O^{18}O^{2-}$	66	7.91619E− 09	$H_2{}^{12}C^{18}O\ {}^{18}O^{18}O$	$^{12}C^{18}\ O^{18}O$	48	1
$^{13}C^{18}O^{18}O^{17}O^{2-}$	66	1.68533E− 11	$H_2{}^{13}C^{18}O\ {}^{18}O^{17}O$	$^{13}C^{18}\ O^{18}O$	49	0.3368476
			$H_2{}^{13}C^{18}O\ {}^{17}O^{18}O$	$^{13}C^{18}\ O^{17}O$	48	0.3309813
			$H_2{}^{13}C^{17}O\ {}^{18}O^{18}O$	$^{13}C^{18}\ O^{17}O$	48	0.3321711
$^{13}C^{18}O^{18}O^{18}O^{2-}$	67	8.89558E− 11	$H_2{}^{13}C^{18}O\ {}^{18}O^{18}O$	$^{13}C^{18}\ O^{18}O$	49	1

[a] Nominal cardinal mass in amu.

[b] Stochastic abundances, i.e., the abundances when all the isotopes are stochastically distributed within the reactant carbonate, with a bulk isotopic composition of $\delta^{13}C_{VPDB} = 0‰$ and $\delta^{18}O_{VSMOW} = 0‰$.

[c] Oxygen atoms in H_2CO_3 intermediate are expressed in the order of atom 2, 3, 4 in Fig. 2, and the last oxygen atoms (atom 4) are the ones to be abstracted during phosphoric acid digestion.

[d] Predicted respective fractions of different product CO_2 isotopologues from the reactant CO_3^{2-} isotopologues at 25 °C, based on our H_2CO_3 model.

$$R_{^{12}C^{18}O^{16}O\text{–}\underline{H_2{}^{16}O^{18}O^{16}O}} = |v_L^{\dagger}|_{\underline{H_2{}^{12}C^{16}O^{18}O^{16}O^{\dagger}}} \times \frac{Q^{\dagger}_{\underline{H_2{}^{12}C^{16}O^{18}O^{16}O^{\dagger}}}}{Q_{\underline{H_2{}^{12}C^{16}O^{18}O^{16}O}}} \times[\underline{H_2{}^{12}C^{16}O^{18}O^{16}O}] \quad (8)$$

$$R_{^{12}C^{16}O_2\text{–}\underline{H_2{}^{16}O^{16}O^{18}O}} = |v_L^{\dagger}|_{\underline{H_2{}^{12}C^{16}O^{16}O^{18}O^{\dagger}}} \times \frac{Q^{\dagger}_{\underline{H_2{}^{12}C^{16}O^{16}O^{18}O^{\dagger}}}}{Q_{\underline{H_2{}^{12}C^{16}O^{16}O^{18}O}}} \times[\underline{H_2{}^{12}C^{16}O^{16}O^{18}O}] \quad (9)$$

where $[\underline{H_2{}^{12}C^{18}O^{16}O^{16}O}]$, $[\underline{H_2{}^{12}C^{16}O^{18}O^{16}O}]$, $[\underline{H_2{}^{12}C^{16}O^{16}O^{18}O}]$ are the abundances of the different isotopomers of $H_2{}^{12}C^{18}O^{16}O_2$ (Fig. 2d–f, respectively). Because the lifetime of carbonic acid is relatively long under anhydrous conditions (Loerting et al., 2000 and reference therein), we assume the concentrations of these various carbonic acid isotopomers are in equilibrium (presumably through the exchanges of protons):

$$\frac{[\underline{H_2{}^{12}C^{18}O^{16}O^{16}O}]}{Q_{\underline{H_2{}^{12}C^{18}O^{16}O^{16}O}}} = \frac{[\underline{H_2{}^{12}C^{16}O^{18}O^{16}O}]}{Q_{\underline{H_2{}^{12}C^{16}O^{18}O^{16}O}}} = \frac{[\underline{H_2{}^{12}C^{16}O^{16}O^{18}O}]}{Q_{\underline{H_2{}^{12}C^{16}O^{16}O^{18}O}}} \quad (10)$$

therefore,

$$R_{^{12}C^{18}O^{16}O\text{–}\underline{H_2{}^{12}C^{18}O^{16}O^{16}O}} : R_{^{12}C^{18}O^{16}O\text{–}\underline{H_2{}^{12}C^{16}O^{18}O^{16}O}} : R_{^{12}C^{16}O_2\text{–}\underline{H_2{}^{12}C^{16}O^{16}O^{18}O}} = (|v_L^{\dagger}| \times Q^{\dagger})_{\underline{H_2{}^{12}C^{18}O^{16}O^{16}O^{\dagger}}} : (|v_L^{\dagger}| \times Q^{\dagger})_{\underline{H_2{}^{12}C^{18}O^{16}O^{16}O^{\dagger}}} : (|v_L^{\dagger}| \times Q^{\dagger})_{\underline{H_2{}^{12}C^{16}O^{16}O^{18}O^{\dagger}}} \quad (11)$$

The relations given above for the case of $H_2{}^{12}C^{18}O^{16}O_2$ are applied to all the isotopologues of H_2CO_3 that are capable of producing more than one CO_2 isotopologue; for H_2CO_3 isotopologues capable of producing only one CO_2 isotopologue, n_i values for that CO_2 isotopologue produced from that H_2CO_3 isotopologue equal n_j of that H_2CO_3 isotopologue, e.g., for isotopologue $H_2{}^{12}C^{16}O_3$, $n_{^{12}C^{16}O_2\text{–}H_2{}^{12}C^{16}O_3} = n_{H_2{}^{12}C^{16}O_3}$. The summation of all n_i values for the various isotopologues of CO_2 produced from all isotopologues of H_2CO_3 allow us to calculate the isotopic fractionations (including the fractionations of multiply substituted isotopologues) associated with acid digestion (Table 1).

2.2.3. Exploration of cation effects during phosphoric acid digestion through cluster models

The cation compositions of carbonate minerals might exert a second-order, but measurable influence on the oxygen isotope fractionation associated with phosphoric acid digestion (e.g., Gilg et al., 2003). The data in support of such effects are open to question, as the fluorination measurements required to independently establish the $\delta^{18}O$ values of reactant carbonates generally have poorer than expected reproducibility (and other peculiarities). Nevertheless, mineral-specific acid digestion fractionations seem possible and are widely assumed. The H_2CO_3-dissociation model we described above cannot account for such effects because it describes carbonic acid, the reaction intermediate, as free isolated molecules without any interactions with the cations present in the carbonate mineral (Section 2.2.1). Thus, while our approach has the advantage of allowing for a relatively rigorous treatment of part of the acid digestion process, it is an over-simplification that will not permit full understanding of differences in fractionations between various types of carbonate minerals. We have tried to develop an understanding of these second-order effects by constructing a 'cluster model' that describes the dissociation of H_2CO_3 attached to XCO_3 clusters, which simulates the situation where H_2CO_3 is influenced by bonds on the surface of adjacent, un-reacted carbonate. Similar ab initio cluster models have been used previously to investigate local properties and reactions of carbonate surfaces, such as hydration (Mao and Siders, 1997) and adsorption (Ruuska et al., 1999). In this study, we limit our model to small clusters comprising only two XCO_3 units, i.e. $(XCO_3)_2 \cdot H_2CO_3$, where $X = Mg^{2+}$, Ca^{2+}, Mn^{2+}, Fe^{2+}, Zn^{2+}, Sr^{2+}, Pb^{2+}, Ba^{2+}.

Following the same method outlined in previous sections, we obtain the structures of the transition states for these clusters (Fig. 3) and derive the isotope fractionations during phosphoric acid digestion of different carbonate minerals. Note, we will confine our discussion on this cluster model to Section 4.4. In other parts of the text, "model" refers to the H_2CO_3 dissociation model described in Section 2.2.1, unless stated otherwise.

2.3. Computational methods

Molecular geometries were optimized and bond frequencies were calculated for the transition state isotopologues using the Jaguar program (Ringnalda et al., 2005), on a workstation cluster with 79 Dell PowerEdge-2650 server nodes (Xeno, 2.2–2.4 GHz, 512 K) in the Materials and Process Simulation Center at Caltech. The singlet state electron wave functions of the molecular configurations were built using a density functional theory with hybrid functionals, B3LYP, and extended basis sets 6–31G* (for the H_2CO_3 model) and LACV3P (for the cluster model). These were selected based on their previous success in similar ab initio models (Foresman and Frisch, 1993; Scott and Radom, 1996; Ringnalda et al., 2005).

Ab initio harmonic oscillator calculations typically overestimate vibration frequencies, mostly because they neglect the effects of anharmonicity (Scott and Radom, 1996). Therefore, a scaling factor based on the comparison between the calculated bond vibration frequencies and experimentally measured frequencies usually needs to be applied to harmonic frequencies derived from ab initio models. No experimentally-measured frequencies of the assumed carbonic acid transition state are available for comparison with our ab initio model. Therefore, we have used a universal frequency scaling factor of 0.9614, previously shown to be appropriate for B3LYP/6-31G* calculations (Scott and Radom, 1996). To test the effectiveness of this assumed frequency scaling factor, we computed the vibration frequencies for the carbonic acid molecule using the B3LYP/6-31G* method, applied the 0.9614 scaling factor, and compared the scaled bond-vibration frequencies to the previously published results (Tossell, 2006) from more sophisticated, higher level calculations (CCSD/6-311+G(2d,p) level) and anharmonicity corrections (B3LYP/CBSB7 level). Results from these two independent models are generally consistent with each other (Fig. 4), suggesting that

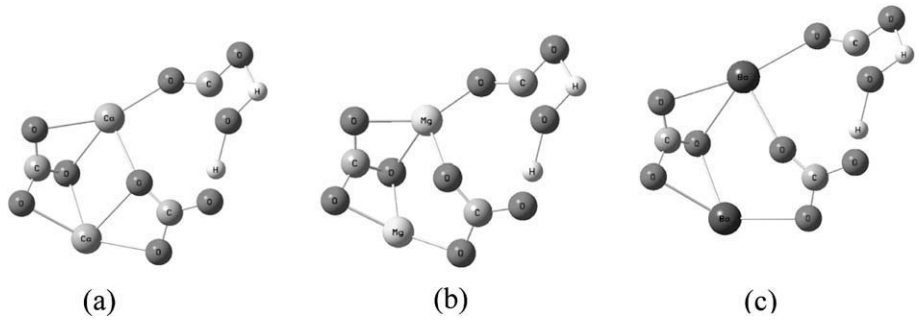

Fig. 3. Representative transition state structures during phosphoric acid digestion of carbonate minerals, as in our 'cluster models' that attempt to describe interactions between disassociating H_2CO_3 and adjacent mineral surfaces. Individual structures are: (a) $(CaCO_3)_2 \cdot H_2CO_3$; (b) $(MgCO_3)_2 \cdot H_2CO_3$; and (c) $(BaCO_3)_2 \cdot H_2CO_3$. Letters denote the chemical identity of each atom.

our scaling of the B3LYP/6-31G* model adequately accounts for systematic errors due to anharmonicity and related effects. No frequency scaling was employed for the cluster model calculations, due to the absence of a universal scaling factor for the LACV3P basis set. However, we show below that any influence of the scaling factor is likely to be negligible for the general conclusions we reach based on our cluster model.

3. EXPERIMENTAL METHODS

Starting materials for the carbonate recrystallization experiments conducted as part of this study consisted of three different calcite materials: NBS19 carbonate standard distributed from IAEA (1 aliquot); MZ carbonate preheated at 1100 °C from Ghosh et al., 2006 (1 aliquot); and Sigma-carb purchased from Sigma–Aldrich Co. (2 aliquots). The materials were loaded into Pt capsules, which were then sealed by welding and inserted into CaF_2 cell assemblies. The experiments were conducted in a piston-cylinder apparatus at 1550 or 1650 °C and either 2 or 3 GPa for 24 h (Table 2). Temperature was monitored using type C thermocouples, uncorrected for the effect of pressure on the electromotive force of the thermocouples. The temperature and pressure conditions were chosen to be close to or above the melting point of $CaCO_3$ (Suito et al., 2001) to ensure complete stochastic distributions of isotopes (which might not occur over laboratory timescales due to solid-state recrystallization alone; Ghosh et al., 2006). Experimental charges were quenched rapidly by turning off the power to the furnace, resulting in cooling to below 200 °C in less than 20 s and to room temperature within 1 minute. Carbonate crystals were recovered by carefully stripping off the Pt capsule. The phase of each sample was verified using X-ray diffraction, and the aliquots were then reacted with anhydrous phosphoric acid ($\rho = 1.91$ g/cm^3) at 25 °C for 18–24 h. The Δ_{47} values of released CO_2 were analyzed on a gas source mass spectrometer configured to simultaneously measure masses 44 to 49. A detailed description of the mass spectrometer configuration and analysis procedures was given by Ghosh et al. (2006).

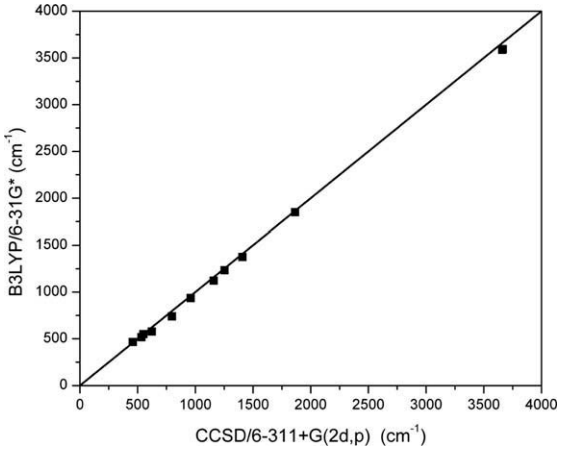

Fig. 4. Comparison of vibration frequencies of gas-phase carbonic acid (H_2CO_3) obtained in this study using B3LYP/6-31G* ab initio models with a scaling factor of 0.9614 vs. those obtained through more sophisticated higher level calculations and anharmonicity corrections (CCSD/6-311+G(2d,p) with B3LYP/CBSB7 based anharmonic calculations and corrections; Tossell, 2006). The solid line indicates a 1:1 correlation.

4. RESULTS AND DISCUSSION

4.1. Experimentally determined acid-digestion fractionation of Δ_{47}

We assume that heating $CaCO_3$ to temperatures and pressures above its melting point should drive its ^{13}C and ^{18}O toward a stochastic distribution. Thus, we anticipate that the Δ_{47} value of the CO_2 extracted from $CaCO_3$ that has been quenched from melt should equal 0 (the stochastic value) plus any fractionation associated with phosphoric acid digestion. There is no simple way for us prove that the stochastic distribution in carbonate is preserved during rapid quenching from a melt, but this seems like a reasonable inference given previous evidence that isotopic redistribution in crystalline calcite is inefficient at laboratory timescales, even at high temperature (Ghosh et al., 2006). X-ray diffraction analyses confirmed that $CaCO_3$ samples quenched from heating experiments are all of the calcite structure. The Δ_{47} values of CO_2 gases derived from these $CaCO_3$ samples average $0.232 \pm 0.015‰$ (1σ), and show no systematic difference between the experiments at 1550 °C/2 Gpa and at 1650 °C/3 Gpa, nor any correlation with the Δ_{47} values of the CO_2 extracted from these samples before recrystalization (Table 2). Note, such a correlation

Table 2
Fractionation of multiply-substituted isotopologues, Δ^*_{47} (see text for the definition), during phosphoric acid digestion of $CaCO_3$ at 25 °C determined through phosphoric acid digestion of high temperature and pressure equilibrated $CaCO_3$ (calcite) samples.

Sample	Before re-crystallization			Re-crystallization experiments			After re-crystallization			
	Δ_{47} (‰)	$\delta^{13}C_{VPDB}$ (‰)	$\delta^{18}O_{VSMOW}$ (‰)	T (°C)	P (GPa)	Duration (h)	Δ_{47} (‰)	1σ[a]	$\delta^{13}C_{VPDB}$ (‰)	$\delta^{18}O_{VSMOW}$ (‰)
Re-crystallized MZ	0.267	−13.66	34.61	1550	2	24	0.234	0.025(3)	−17.03	34.11
NBS19 standard	0.334	2.01	39.28	1550	2	24	0.210	0.012(2)	−4.82	38.64
Sigma carbonate	0.468	−42.28	20.55	1550	2	24	0.243	0.015(3)	−33.96	20.44
				1650	3	24	0.239	0.009(2)	−25.82	20.78

[a] 1σ denotes the external standard deviation. Numbers in the bracket indicate the numbers of independent replicate extraction and isotopic analyses of the carbonate samples after re-crystallization.

was observed by Ghosh et al. (2006), in the products of solid-state recrystallization experiments, leading them to conclude that such treatment led to only partial approach to the stochastic distribution. These results support our inference that our heating experiments succeeded at driving these samples to a stochastic distribution, and thus imply that the 'clumped isotope' fractionation of ^{13}C–^{18}O bonds during phosphoric acid digestion of calcite at 25 °C corresponds to an increase in Δ_{47} of 0.23‰ in product CO_2.

4.2. Model results for the oxygen-isotope and clumped-isotope fractionations associated with phosphoric acid digestion

Table 3 summarizes the vibration frequencies we calculate for the various isotopologues and isotopomers of transition states in our H_2CO_3 dissociation model. The negative frequencies, ϖ_1, correspond to the decomposition frequencies $\nu_L^\dagger$ in Section 3.1 (Melander and Saunders, 1987). Following procedures outlined in Section 3, these frequencies are used in our transition-state-based predictions of the proportions of different CO_2 isotopologues that are produced by dissociation of the H_2CO_3 intermediate, and the temperature dependence of those proportions. Unless stated otherwise, all of our calculations assume that reactant carbonate has a $\delta^{13}C_{VPDB}$ value of 0‰, a $\delta^{18}O_{VSMOW}$ value of 0‰ and a stochastic distribution of multiply-substituted isotopologues (Table 1), and that the H_2CO_3 intermediate is identical in isotopic composition to reactant carbonate (Section 2.2.2).

We define the fractionations of oxygen isotope ($1000\ln\alpha^*$) and multiply substituted species ($\Delta^*_{47}, \Delta^*_{48}, \Delta^*_{49}$) during phosphoric acid digestion as the differences between $\delta^{18}O$, Δ_{47}, Δ_{48}, Δ_{49} in the product CO_2 and $\delta^{18}O$, Δ_{63},Δ_{64},Δ_{65} in the reactant carbonates, respectively:

$$1000\ln\alpha^* = 1000\ln\frac{\delta^{18}O_{CO_2}/1000+1}{\delta^{18}O_{XCO_3}/1000+1},$$

$$\Delta^*_{47} = \Delta_{47} - \Delta_{63}, \quad \Delta^*_{48} = \Delta_{48} - \Delta_{64}, \quad \Delta^*_{49} = \Delta_{49} - \Delta_{65}$$

where Δ_{48}, Δ_{49}, Δ_{63}, Δ_{64} and Δ_{65} are defined, similar to Δ_{47}, following the same principle as in Eiler and Schauble (2004):

$$\Delta_{48} = \left(\frac{R^{48}_{actual}}{R^{48}_{stochastic}} - 1\right) \times 1000 = \left(\frac{\frac{[^{12}C^{18}O^{18}O]+[^{13}C^{18}O^{17}O]}{[^{12}C^{16}O^{16}O]}}{\frac{[^{12}C^{18}O^{18}O]_s+[^{13}C^{18}O^{17}O]_s}{[^{12}C^{16}O^{16}O]_s}} - 1\right) \times 1000; \quad (12)$$

$$\Delta_{49} = \left(\frac{R^{49}_{actual}}{R^{49}_{stochastic}} - 1\right) \times 1000 = \left(\frac{\frac{[^{13}C^{18}O^{18}O]}{[^{12}C^{16}O^{16}O]}}{\frac{[^{13}C^{18}O^{18}O]_s}{[^{12}C^{16}O^{16}O]_s}} - 1\right) \times 1000; \quad (13)$$

$$\Delta_{63} = \left(\frac{R^{63}_{actual}}{R^{63}_{stochastic}} - 1\right) \times 1000 = \left(\frac{\frac{[X^{13}C^{18}O^{16}O]+[X^{12}C^{18}O^{17}O^{16}O]+[X^{13}C^{17}O^{17}O^{16}O]+[X^{12}C^{17}O^{17}O^{17}O]}{[X^{12}C^{16}O^{16}O^{16}O]}}{\frac{[X^{13}C^{18}O^{16}O^{16}O]_s+[X^{12}C^{18}O^{17}O^{16}O]_s+[X^{13}C^{17}O^{17}O^{16}O]_s+[X^{12}C^{17}O^{17}O^{17}O]_s}{[X^{12}C^{16}O^{16}O^{16}O]_s}} - 1\right) \times 1000; \quad (14)$$

$$\Delta_{64} = \left(\frac{R^{64}_{actual}}{R^{64}_{stochastic}} - 1\right) \times 1000 = \left(\frac{\frac{[X^{12}C^{18}O^{18}O^{16}O]+[X^{13}C^{18}O^{17}O^{16}O]+[X^{12}C^{18}O^{18}O^{17}O]+[X^{13}C^{17}O^{17}O^{17}O]}{[X^{12}C^{16}O^{16}O^{16}O]}}{\frac{[X^{12}C^{18}O^{18}O^{16}O]_s+[X^{13}C^{18}O^{17}O^{16}O]_s+[X^{12}C^{18}O^{18}O^{17}O]_s+[X^{13}C^{17}O^{17}O^{17}O]_s}{[X^{12}C^{16}O^{16}O^{16}O]_s}} - 1\right) \times 1000; \quad (15)$$

$$\Delta_{65} = \left(\frac{R^{65}_{actual}}{R^{65}_{stochastic}} - 1\right) \times 1000 = \left(\frac{\frac{[X^{12}C^{18}O^{18}O^{17}O]+[X^{13}C^{18}O^{18}O^{16}O]+[X^{13}C^{18}O^{17}O^{17}O]}{[X^{12}C^{16}O^{16}O^{16}O]}}{\frac{[X^{12}C^{18}O^{18}O^{17}O]_s+[X^{13}C^{18}O^{18}O^{16}O]_s+[X^{13}C^{18}O^{17}O^{17}O]_s}{[X^{12}C^{16}O^{16}O^{16}O]_s}} - 1\right) \times 1000; \quad (16)$$

where '*s*' in the subscript denotes the expected abundance of an isotopologue when all the isotopes are stochastically distributed; and X denotes the cation contained in the carbonate mineral.

Fig. 5 and Table 4 present the oxygen isotope fractionations that accompany phosphoric acid digestion over a range of relevant temperatures, as predicted by our transition-state theory model. The predicted oxygen isotope fractionation and its temperature dependence are broadly similar to those determined for different carbonate minerals in previous laboratory studies. At 25 °C, our model predicted oxygen isotope fractionation of 10.72‰, is in the middle of the range of observed fractionations among different carbonate minerals (from 10.06‰ for $MnCO_3$ to 11.92‰ for $MgCO_3$), and is close to the experimental

Table 3
Scaled vibration frequencies (unit: cm^{-1}) for different transition state structure isotopomers during phosphoric acid digestion of carbonate minerals (H_2CO_3 model, DFT-B3LYP/6-31G* with a frequency scaling factor of 0.9614). Oxygen atoms in the transition state structure isotopomers are expressed in the order of atom 2, 3 and 4 in Fig. 2.

Isotopomer	ϖ_1	ϖ_2	ϖ_3	ϖ_4	ϖ_5	ϖ_6	ϖ_7	ϖ_8	ϖ_9	ϖ_{10}	ϖ_{11}	ϖ_{12}
$H_2{}^{12}C^{16}O^{16}O^{16}O^{\dagger}$	−1650.22	381.74	489.85	588.65	720.73	760.00	927.16	1246.50	1267.18	1903.52	2102.57	3573.50
$H_2{}^{13}C^{16}O^{16}O^{16}O^{\dagger}$	−1643.59	380.77	488.29	577.55	710.57	754.21	920.93	1234.69	1266.94	1881.48	2069.33	3573.50
$H_2{}^{12}C^{17}O^{16}O^{16}O^{\dagger}$	−1649.47	381.07	489.52	587.30	716.91	750.19	925.95	1230.07	1266.52	1901.17	2101.66	3573.50
$H_2{}^{12}C^{16}O^{17}O^{16}O^{\dagger}$	−1650.10	378.19	488.88	587.13	719.09	755.13	926.78	1237.11	1266.92	1896.67	2094.47	3573.50
$H_2{}^{12}C^{16}O^{16}O^{17}O^{\dagger}$	−1649.38	377.05	487.91	587.36	713.34	757.87	924.34	1246.34	1265.39	1902.99	2102.51	3567.31
$H_2{}^{12}C^{18}O^{16}O^{16}O^{\dagger}$	−1648.80	380.42	489.21	586.08	713.11	741.52	924.84	1215.38	1265.98	1899.15	2100.89	3573.50
$H_2{}^{12}C^{16}O^{18}O^{16}O^{\dagger}$	−1649.99	374.93	488.00	585.78	717.47	750.72	926.43	1228.35	1266.80	1890.27	2087.85	3573.50
$H_2{}^{12}C^{16}O^{16}O^{18}O^{\dagger}$	−1648.64	372.65	486.21	586.06	706.41	756.43	921.86	1246.19	1263.81	1902.53	2102.45	3561.83
$H_2{}^{13}C^{17}O^{16}O^{16}O^{\dagger}$	−1642.83	380.13	488.01	576.12	707.41	744.04	919.75	1217.63	1266.31	1878.83	2068.74	3573.50
$H_2{}^{13}C^{16}O^{17}O^{16}O^{\dagger}$	−1643.46	377.27	487.23	576.01	708.42	750.10	920.55	1225.28	1266.72	1872.20	2063.05	3573.50
$H_2{}^{13}C^{16}O^{16}O^{17}O^{\dagger}$	−1642.75	376.08	486.35	576.41	704.07	751.04	918.05	1234.52	1265.14	1881.01	2069.22	3567.30
$H_2{}^{12}C^{17}O^{17}O^{16}O^{\dagger}$	−1649.35	377.52	488.56	585.76	715.41	745.12	925.59	1220.74	1266.33	1894.08	2093.59	3573.50
$H_2{}^{12}C^{17}O^{16}O^{17}O^{\dagger}$	−1648.63	376.41	487.58	585.96	709.09	748.37	923.15	1229.93	1264.71	1900.64	2101.59	3567.31
$H_2{}^{12}C^{16}O^{17}O^{17}O^{\dagger}$	−1649.26	373.46	486.96	585.84	711.98	752.68	923.96	1236.95	1265.12	1896.15	2094.39	3567.31
$H_2{}^{13}C^{18}O^{16}O^{16}O^{\dagger}$	−1642.14	379.51	487.73	574.82	704.33	734.92	918.66	1202.37	1265.78	1876.56	2068.24	3573.50
$H_2{}^{13}C^{16}O^{18}O^{16}O^{\dagger}$	−1643.34	374.05	486.27	574.66	706.31	746.40	920.21	1216.51	1266.59	1863.66	2058.04	3573.50
$H_2{}^{13}C^{16}O^{16}O^{18}O^{\dagger}$	−1642.00	371.68	484.64	575.27	697.76	748.85	915.50	1234.38	1263.55	1880.60	2069.11	3561.83
$H_2{}^{12}C^{18}O^{17}O^{16}O^{\dagger}$	−1648.68	376.86	488.26	584.53	711.79	736.22	924.50	1206.14	1265.81	1891.85	2092.85	3573.50
$H_2{}^{12}C^{18}O^{16}O^{17}O^{\dagger}$	−1647.96	375.78	487.27	584.69	704.84	740.04	922.07	1215.25	1264.17	1898.62	2100.82	3567.30
$H_2{}^{12}C^{17}O^{18}O^{16}O^{\dagger}$	−1649.24	374.25	487.71	584.41	713.89	740.56	925.26	1212.10	1266.21	1887.46	2087.00	3573.50
$H_2{}^{12}C^{17}O^{16}O^{18}O^{\dagger}$	−1647.89	372.02	485.88	584.61	701.79	747.20	920.69	1229.81	1263.12	1900.18	2101.54	3561.83
$H_2{}^{12}C^{16}O^{18}O^{17}O^{\dagger}$	−1649.15	370.15	486.11	584.50	710.69	747.92	923.62	1228.19	1265.00	1889.76	2087.76	3567.31
$H_2{}^{12}C^{16}O^{17}O^{18}O^{\dagger}$	−1648.51	369.01	485.28	584.55	705.19	751.07	921.48	1236.82	1263.53	1895.70	2094.33	3561.83
$H_2{}^{13}C^{17}O^{17}O^{16}O^{\dagger}$	−1642.70	376.62	486.96	574.56	705.29	739.84	919.39	1208.33	1266.13	1869.28	2062.50	3573.50
$H_2{}^{13}C^{17}O^{16}O^{17}O^{\dagger}$	−1641.99	375.46	486.07	574.94	700.60	741.04	916.89	1217.48	1264.51	1878.36	2068.62	3567.30
$H_2{}^{13}C^{16}O^{17}O^{17}O^{\dagger}$	−1642.62	372.53	485.31	574.88	702.27	746.55	917.68	1225.12	1264.92	1871.74	2062.91	3567.30
$H_2{}^{12}C^{17}O^{17}O^{17}O^{\dagger}$	−1648.51	372.80	486.65	584.43	707.89	742.97	922.80	1220.60	1264.52	1893.56	2093.51	3567.30
$H_2{}^{12}C^{18}O^{18}O^{16}O^{\dagger}$	−1648.57	373.59	487.42	583.16	710.40	731.48	924.19	1197.60	1265.70	1885.04	2086.30	3573.50
$H_2{}^{12}C^{18}O^{16}O^{18}O^{\dagger}$	−1647.21	371.41	485.56	583.28	697.20	739.13	919.62	1215.14	1262.56	1898.16	2100.76	3561.82
$H_2{}^{12}C^{16}O^{18}O^{18}O^{\dagger}$	−1648.40	365.67	484.44	583.22	704.07	746.11	921.15	1228.05	1263.40	1889.31	2087.69	3561.83
$H_2{}^{13}C^{18}O^{17}O^{16}O^{\dagger}$	−1642.01	375.99	486.70	573.25	702.27	730.63	918.33	1193.18	1265.62	1866.79	2062.04	3573.50
$H_2{}^{13}C^{18}O^{16}O^{17}O^{\dagger}$	−1641.30	374.86	485.79	573.61	697.17	732.16	915.83	1202.23	1263.98	1876.09	2068.12	3567.30
$H_2{}^{13}C^{17}O^{18}O^{16}O^{\dagger}$	−1642.58	373.39	486.01	573.20	703.17	736.12	919.08	1199.68	1266.01	1860.50	2057.53	3573.50
$H_2{}^{13}C^{17}O^{16}O^{18}O^{\dagger}$	−1641.23	371.07	484.35	573.76	693.95	739.07	914.36	1217.36	1262.91	1877.95	2068.52	3561.82
$H_2{}^{13}C^{16}O^{18}O^{17}O^{\dagger}$	−1642.50	369.27	484.37	573.53	700.54	742.45	917.34	1216.33	1264.79	1863.21	2057.90	3567.30
$H_2{}^{13}C^{16}O^{17}O^{18}O^{\dagger}$	−1641.87	368.09	483.62	573.74	696.18	744.09	915.14	1224.97	1263.33	1871.34	2062.80	3561.82
$H_2{}^{12}C^{18}O^{17}O^{17}O^{\dagger}$	−1647.84	372.17	486.35	583.15	703.81	734.43	921.73	1206.01	1264.00	1891.33	2092.77	3567.30
$H_2{}^{12}C^{17}O^{18}O^{17}O^{\dagger}$	−1648.40	369.49	485.81	583.08	706.73	738.01	922.48	1211.96	1264.41	1886.95	2086.92	3567.30
$H_2{}^{12}C^{17}O^{17}O^{18}O^{\dagger}$	−1647.76	368.38	484.96	583.09	700.72	741.63	920.33	1220.48	1262.93	1893.11	2093.45	3561.83
$H_2{}^{13}C^{17}O^{17}O^{17}O^{\dagger}$	−1641.85	371.91	485.04	573.39	698.92	736.38	916.54	1208.18	1264.33	1868.83	2062.36	3567.30
$H_2{}^{13}C^{18}O^{18}O^{16}O^{\dagger}$	−1641.90	372.76	485.76	571.88	700.13	726.89	918.04	1184.64	1265.50	1857.79	2057.10	3573.50
$H_2{}^{13}C^{18}O^{16}O^{18}O^{\dagger}$	−1640.55	370.49	484.08	572.38	690.16	730.46	913.32	1202.12	1262.38	1875.68	2068.02	3561.82
$H_2{}^{13}C^{16}O^{18}O^{18}O^{\dagger}$	−1641.75	364.78	482.70	572.40	694.69	739.72	914.81	1216.18	1263.20	1862.82	2057.77	3561.82
$H_2{}^{12}C^{18}O^{18}O^{17}O^{\dagger}$	−1647.73	368.85	485.53	581.79	702.81	729.25	921.42	1197.47	1263.89	1884.52	2086.21	3567.30
$H_2{}^{12}C^{18}O^{17}O^{18}O^{\dagger}$	−1647.09	367.76	484.66	581.75	696.27	733.38	919.28	1205.90	1262.40	1890.88	2092.70	3561.82
$H_2{}^{12}C^{17}O^{18}O^{18}O^{\dagger}$	−1647.65	365.03	484.14	581.75	699.73	736.48	920.02	1211.83	1262.81	1886.50	2086.84	3561.82
$H_2{}^{13}C^{18}O^{17}O^{17}O^{\dagger}$	−1641.17	371.29	484.78	572.05	695.63	727.32	915.50	1193.04	1263.82	1866.33	2061.90	3567.30
$H_2{}^{13}C^{17}O^{18}O^{17}O^{\dagger}$	−1641.74	368.63	484.12	572.03	697.26	732.17	916.23	1199.52	1264.21	1860.05	2057.39	3567.30
$H_2{}^{13}C^{17}O^{17}O^{18}O^{\dagger}$	−1641.10	367.48	483.35	572.22	692.51	734.13	914.02	1208.05	1262.73	1868.42	2062.24	3561.82
$H_2{}^{12}C^{18}O^{18}O^{18}O^{\dagger}$	−1646.98	364.40	483.85	580.40	695.42	728.04	918.98	1197.36	1262.30	1884.07	2086.13	3561.82
$H_2{}^{13}C^{18}O^{18}O^{17}O^{\dagger}$	−1641.05	368.01	483.87	570.68	694.07	722.97	915.21	1184.49	1263.70	1857.34	2056.96	3567.30
$H_2{}^{13}C^{18}O^{17}O^{18}O^{\dagger}$	−1640.42	366.88	483.09	570.83	688.88	725.32	913.00	1192.92	1262.22	1865.93	2061.78	3561.82
$H_2{}^{13}C^{17}O^{18}O^{18}O^{\dagger}$	−1640.99	364.17	482.44	570.86	691.14	729.60	913.71	1199.39	1262.62	1859.66	2057.26	3561.82
$H_2{}^{13}C^{18}O^{18}O^{18}O^{\dagger}$	−1640.31	363.56	482.19	569.46	687.64	720.61	912.71	1184.37	1262.10	1856.95	2056.82	3561.82

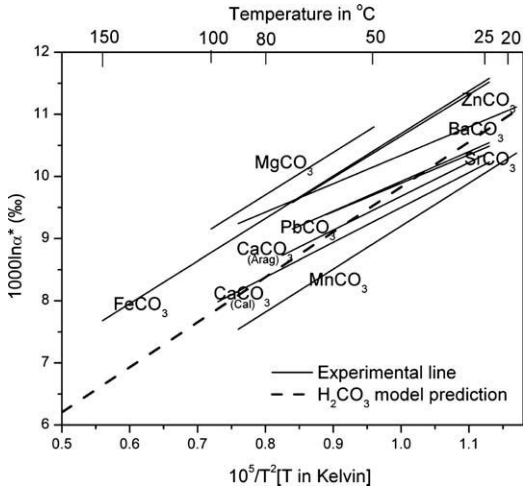

Fig. 5. Oxygen isotope fractionations ($1000\ln\alpha^*$, where α^* is the $^{18}O/^{16}O$ ratio of product CO_2 divided by that of reactant carbonate) plotted vs. 10^5T^{-2} in K (the upper horizontal edge indicates T in °C, for reference). The dashed line is the predicted temperature-dependent fractionation based on our model of H_2CO_3 dissociation. Labeled solid lines are measured experimental values for various metal carbonates (Table 4). The structurally simple transition-state structure model we propose captures the first-order magnitude and temperature dependence of observed fractionations, and mostly closely approaches the best-determined value for calcite.

determined fractionation for calcite (10.20‰). The temperature sensitivity of our predicted oxygen isotope fractionation during phosphoric acid digestion (−0.055‰/°C at 25 °C) is also only slightly above the range of temperature sensitivities experimentally determined for different carbonate minerals ($MnCO_3$ appears to possess the highest temperature sensitivity of oxygen isotope aid digestion fractionation, −0.052‰/°C at 25 °C).

Our transition-state-theory model of phosphoric acid digestion predicts that CO_2 produced by dissociation of H_2CO_3 intermediates has abundances of ^{13}C–^{18}O bonds, as reflected by the Δ^*_{47} value, +0.220‰ higher than the Δ_{63} value of reactant carbonate at 25 °C, with a temperature sensitivity of −0.0010‰/°C over the temperature range of 25 °C to 80 °C. The predicted fractionation at 25 °C is indistinguishable from this study's experimentally determined value of 0.232 ± 0.015‰ (1σ) for calcite (Table 2), and the predicted temperature dependence is close to the experimentally measured value of ca. −0.0016‰/°C (Ghosh et al., 2006). There are no experimental data documenting fractionations of $^{12}C^{18}O_2$ and $^{13}C^{18}O_2$ isotopologues during acid digestion of carbonates, but for future reference we note here that our transition state theory model predicts Δ^*_{48} to be 0.137‰ at 25 °C with a temperature dependence of −0.0011‰/°C, and Δ^*_{49} to be 0.593‰ at 25 °C with a temperature dependence of −0.0033‰/°C (Fig. 6).

The most obvious weakness of our transition state theory model is the need to choose a frequency scaling factor (which mainly reflects the effects of anharmonicity; see Section 2.3, above). We tested the potential effects of this frequency scaling by repeating our calculations with no scaling factors. In this case, the predicted acid digestion fractionations at 25 °C are 11.32‰ for $1000\ln\alpha^*$, 0.235‰ for Δ^*_{47}, 0.156‰ for Δ^*_{48}, and 0.642‰ for Δ^*_{49}. These results are sufficiently similar to the results of our preferred model that we do not regard the frequency scaling factors as plausible sources of large systematic error.

Our transition state theory model also predicts the mass dependency of the oxygen isotope fractionation that accompanies phosphoric acid digestion. This is relevant for analyses of the isotopic compositions of reactant carbonates because one must assume the mass dependence of the acid digestion fractionation in order to ion-correct the measured mass spectrum of product CO_2. Generally speaking, measurements of the carbon and oxygen isotope compositions of CO_2 on a gas source isotope ratio mass spectrometer examine CO_2 isotopologue ions having nominal molecular masses of 44, 45 and 46 amu. Because the instruments commonly used for this purpose cannot mass resolve $^{13}C^{16}O_2$ from $^{12}C^{17}O^{16}O$, one must make some assumptions to correct for the contribution of $^{12}C^{17}O^{16}O$ to the mass 45 amu ion beam. This is generally accomplished by assuming a relationship between ^{17}O and ^{18}O abundance of the form: $\frac{^{17}R_A}{^{17}R_B} = \left(\frac{^{18}R_A}{^{18}R_B}\right)^{\lambda}$ (Assonov and Brenninkmeijer, 2003; Miller et al., 2007), where the value λ must be assumed or determined by independent experiments (such as fluorination of reactant carbonate and product CO_2 followed by isotopic analyses of the resulting O_2 gases). To the best of our knowledge, there are no experimental determinations of λ associated with phosphoric acid digestion of carbonate minerals; a value 0.528 has been suggested (Assonov and Brenninkmeijer, 2003; Miller et al., 2007). This value of λ characterizes the isotopic variations of natural waters (Li and Meijer, 1998; Barkan and Luz, 2005), and presumably is inherited by carbonate minerals that form in isotopic equilibrium with natural waters, although there is no reason to suppose it is also characteristic of the acid digestion reaction process by which carbonates are analyzed. Our transition state theory of phosphoric acid digestion predicts that the value of λ associated with its isotopic fractionations is 0.5281. Thus, our model agrees with and provides an independent theoretical justification for the suggested value of 0.528 for CO_2 extracted from carbonate samples (Miller et al., 2007) and standards (e.g. PDB and NBS-19; Assonov and Brenninkmeijer, 2003). This result may be useful for the interpretation of high-precision measurements of ^{17}O-anomalies in natural carbonates by fluorinating CO_2 that is generated by phosphoric acid digestion.

4.3. Dependence of acid digestion fractionations on the isotopic compositions of reactant carbonate minerals?

In a recent experimental determinations of oxygen isotope fractionations associated with phosphoric acid digestion, Kim and O'Neil's, 1997 observed apparent variations of the fractionation factors within a single type of carbonate minerals at a single temperature (25 °C): up to 0.5‰ for calcite ($CaCO_3$), 0.6‰ for witherite ($BaCO_3$), and 2.5‰ for octavite ($CdCO_3$). While Kim and O'Neil (1997) suggested

Table 4
Comparison of model predicted and experimentally observed phosphoric acid digestion fractionations.

Carbonate minerals		$\delta^{18}O_{SMOW}$[a] (‰,XCO_3)	Temperature range (°C)	$1000\ln\alpha^*$ (‰[b])	$1000\ln\alpha^*$ (‰, 25. °C[b])	Δ^*_{47} (‰, 25 °C[d])	$1000\ln\alpha^*$ Reference
Calcite group	Dolomite($CaMg(CO_3)_2$)	11.53	25	N/A	11.03	0.214	Sharma and Clayton, 1965
	Magnesite($MgCO_3$)	18.23	50–100	$4.23 + 6.84 \times 10^5/T^2$	11.92	0.198	Das Sharma et al., 2002
	Simthsonite($ZnCO_3$)	26.01	25–72	$3.96 + 6.69 \times 10^5/T^2$	11.49	0.205	Gilg et al., 2003
	Siderite($FeCO_3$)	4.22	25–150	$3.85 + 6.84 \times 10^5/T^2$	11.54	0.204	Rosenbaum and Sheppard, 1986
	Rhodochrosite($MnCO_3$)	18.15	20–90	$2.29 + 6.91 \times 10^5/T^2$	10.06	0.234	Bottcher, 1996
	Calcite($CaCO_3$)	6.43	25–95	$3.89 + 5.61 \times 10^5/T^2$	10.20	0.231	Das Sharma et al., 2002
Aragonite group	Aragonite($CaCO_3$)	25.02	25–75	$4.24 + 5.44 \times 10^5/T^2$	10.36	0.229	Recalculated from Kim et al. 2007[c]
	Strontianite($SrCO_3$)	14.57	25–62	$5.30 + 4.59 \times 10^5/T^2$	10.46	0.225	Sharma and Sharma, 1969a
	Cerussite($PbCO_3$)	15.97	25–72	$5.13 + 4.79 \times 10^5/T^2$	10.52	0.224	Gilg et al., 2003
	Witherite($BaCO_3$)	6.20	20–90	$5.76 + 4.58 \times 10^5/T^2$	10.91	0.216	Bottcher, 1996
H_2CO_3 Model[e]	$1000\ln\alpha^*$	0		$2.58 + 7.25 \times 10^5/T^2$	10.72		This work
	Δ^*_{47}			$0.0186 + 0.179 \times 10^5/T^2$	0.220		This work
	Δ^*_{48}			$-0.0787 + 0.192 \times 10^5/T^2$	0.137		This work
	Δ^*_{49}			$-0.0386 + 0.561 \times 10^5/T^2$	0.593		This work

[a] Oxygen isotope compositions of the reactant carbonate minerals employed in different experimental studies.

[b] Equations for experimentally determined oxygen isotope phosphoric acid digestion fractionation, as summarized in Gilg et al., 2003, where T is in the unit of Kelvin. Isotope fractionations at 25 °C are estimated from these equations.

[c] The oxygen isotope composition of the reactant aragonite was recalculated at 100% total oxygen yield, to account for the inverse correlation between the total oxygen isotopic composition of reactant aragonite and the total oxygen yield from decarbonation and fluorination steps ($\delta^{18}O_{aragonite} = -0.1362 \times Yield\% + 38.642$, Fig. 2 and Table 4 in Kim et al., 2007). The aragonite phosphoric acid digestion fractionations were adjusted accordingly.

[d] Predicted Δ^*_{47} for different carbonate minerals at 25 °C, based on the inverse correlation between $1000\ln\alpha^*$ and Δ^*_{47} predicted by our cluster model. See Section 4.4.3 for details.

[e] Calculations in our H_2CO_3 dissociation model assumes $\delta^{13}C_{VPDB} = 0‰$, $\delta^{18}O_{VSMOW} = 0‰$ and stochastic distribution of multiply-substituted isotopologues for the reactant carbonate.

these effects might be related to differences in the preparation conditions of those carbonates, we are not aware of any detailed explanation that has been put forward for the observed variations.

We performed a statistical analysis of the experimental data presented in Kim and O'Neil (1997), and observed statistically significant correlations between the oxygen isotope acid digestion fractionations and the oxygen isotope compositions of the reactant carbonates, with proportionalities of: 0.03‰ change in fractionation per permil in reactant $\delta^{18}O$ for calcite; 0.036‰ per permil for octavite; and 0.06 ‰ per permil for witherite (Fig. 7). Interestingly, we find these observed correlations might help explain some of the discrepancies between independent determinations of acid digestion fractionation factors, e.g., for octavite and calcite in Kim and O'Neil, 1997 and Sharma and Clayton (1965) (Fig. 7). However, the discrepancy between these two studies in the acid digestion fractionation for witherite cannot be explained in this way (Fig. 7).

The possibility that acid digestion fractionations depend on $\delta^{18}O$ of the reactant carbonate is generally neglected in studies of carbonate stable isotope composition, though the existence of such an effect could lead to significant systematic errors for some materials. We examined this issue by recalculating our transition state theory model for a range of bulk isotopic compositions and initial multiply-substituted isotopologue proportions (i.e., values of Δ_{63}, Δ_{64}, etc.) in the reactant carbonate (assumed identical to H_2CO_3 intermediate) at a constant assumed acid digestion temperature of 25 °C (Table 5). The proportions of multiply substituted isotopologues inside reactant carbonate are calculated based on the equilibrium constants of isotope exchange reactions between different carbonate ion isotopologues, following the similar algorithm as presented in Wang et al. (2004) (see Appendix A-1 for details).

We observe no dependence of the oxygen isotope acid digestion fractionation ($1000\ln\alpha^*$) on the $\delta^{18}O$ value of the reactant carbonate, and thus our model does not provide an explanation of such trends in the experimental data of Kim and O'Neil (1997). Given the general success of our model in describing the magnitude and temperature dependence of $1000\ln\alpha^*$ (Fig. 5), this discrepancy likely indicates that the trends observed by Kim and O'Neil (Fig. 7) are not an intrinsic feature of the kinetic isotope effect that accompanies phosphoric acid digestion of carbonate. Such trends might instead reflect systematic errors in the fluorination measurements that were used to determine the bulk $\delta^{18}O$ of reactant carbonates (e.g., as might result from an unrecognized analytical blank or contaminant), or, as suggested by Kim and O'Neil (1997), some cryptic artifact particular to the synthesis of the carbonate materials they studied.

However, the transition-state-theory models summarized in Table 5 show an unexpected dependence of the fractionations of multiply-substituted isotopologues (i.e., values of Δ^*_{47}, Δ^*_{48} and Δ^*_{49}) on proportions of multiply substituted isotopologues of reactant carbonates (i.e., values of Δ_{63}, Δ_{64} and Δ_{65}). Most importantly, Δ^*_{47}, the fractionation that directly influences the results of carbonate clumped isotope thermometry, is predicted to increase by ~0.035‰ for every 1‰ increase in the Δ_{63} value of reactant carbonate. This non-ideality in the clumped isotope fractionations arises from a peculiarity in the way the Δ_i values are defined (see Appendix A-2 for details).

The available experimental data do not directly test our predicted dependence of Δ^*_{47} on Δ_{63} of reactant carbonate. However, the predicted effect does offer a partial explana-

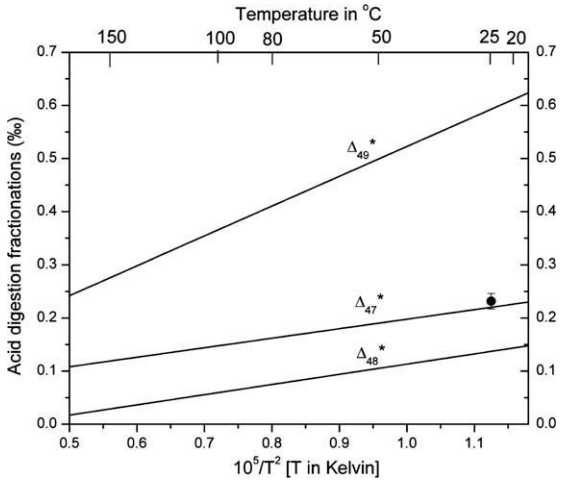

Fig. 6. Fractionations of multiply-substituted species (Δ_{47}^*, Δ_{48}^*, Δ_{49}^*) during phosphoric acid digestion predicted by our H_2CO_3 dissociation model, plotted as a function of 10^5T^{-2}, in K. The solid circle is the average value of Δ_{47}^* experimentally determined during phosphoric acid digestion of calcites at 25 °C (Table 2; this study). The bar is 1 standard deviation (1σ) of multiple replicate extractions of the calcites (the standard error of the average is approximately the size of the symbol).

tion why the experimentally determined relationship between the Δ_{47} of CO_2 produced by acid digestion of calcite and calcite growth temperature (Ghosh et al., 2006) is more sensitive to temperature than the theoretically predicted temperature dependence for Δ_{63} in carbonates (Schauble et al., 2006). For example, over the temperature range of 0–50 °C, Schauble et al. (2006) predicts Δ_{63} (including contributions from both $\Delta_{^{13}C^{18}O^{16}O_2}$ and $\Delta_{^{12}C^{18}O^{17}O^{16}O}$; see Appendix A-2) in thermodynamically equilibrated calcite solids decreases by 0.00279‰ for every degree increase of its growth temperature; Assuming calcite has the same dependence of Δ_{47}^* on Δ_{63} as predicted by our above H_2CO_3 model, we predict the Δ_{47} of CO_2 produced by acid digestion of calcite will have a temperature sensitivity of −0.00289‰/°C, which is closer to the −0.00453‰/°C determined experimentally by Ghosh et al. (2006) than the theoretically predicted temperature sensitive of Δ_{63} (Schauble et al., 2006).

4.4. Cation effects on acid digestion fractionations

The transition-state model we present in preceding sections simultaneously explains a variety of features of the kinetic isotope effects associated with phosphoric acid digestion of carbonates, including the magnitude and temperature dependence of $1000\ln\alpha^*$ and Δ_{47}^* fractionations. Given that all of these predictions are strictly independent of the experimental data to which they are compared, we contend that our model closely captures the most important mechanistic details of this reaction. However, phosphoric acid digestion of carbonates is also believed to exhibit a dependence of $1000\ln\alpha^*$ on the cation chemistry (and possibly crystal structure) of reactant carbonate (Table 4; Fig. 5). At 25 °C, the observed oxygen isotope fractionations among different carbonate minerals vary from 10.06‰ ($MnCO_3$) to 11.92‰ ($MgCO_3$), and the temperature sensitivity of oxygen isotope fractionations during phosphoric acid digestion vary from −0.027‰/°C ($BaCO_3$) to −0.041‰/°C ($MnCO_3$) over the temperature range of 25 °C to 80 °C (Table 4; Fig. 5). Nothing in our above model of H_2CO_3 dissociation can explain such observations. In this section, we use a cluster model of the reacting carbonate surface (Section 2.2.3 and Fig. 3) to explore the possible causes of these effects.

4.4.1. Cluster model results on the oxygen isotope fractionation among different carbonate minerals

Table 6 and Fig. 8 present the predictions of our cluster model on the variations of oxygen isotope fractionation among different carbonate minerals, and the comparisons between these cluster model predictions and the results determined from previous experimental studies. Our cluster model of the carbonate surface, in which the H_2CO_3 intermediate interacts with adjacent metal-carbonate groups, succeeds in capturing the experimentally-observed dependence of $1000\ln\alpha^*$ on cation composition, but fails to describe the absolute values and absolute temperature dependences of $1000\ln\alpha^*$(and Δ_{47}^*) characteristic of our simpler H_2CO_3 dissociation model (above).

In particular, our cluster model predicts values of $1000\ln\alpha^*$ at 25 °C from 1.771‰ ($PbCO_3$) to 3.652‰ ($FeCO_3$) for the eight different carbonate minerals studied (Table 6). Except for $PbCO_3$, these predicted oxygen isotope fractionations are approximately one-third the experimentally observed values. Nevertheless, the predicted differences in oxygen isotope fractionation between different minerals generally reproduce those observed in previous experimental studies (Fig. 8a). The oxygen isotope fractionation predicted by our cluster model for $PbCO_3$ is an exception, falling far below the trend defined by other carbonate minerals. This might be related to the spin-orbit effects and the basis set superposition error in ab initio calculations of Pb-containing complexes with effective core potential basis sets (Ramirez et al., 2006). We evaluate the temperature sensitivity of oxygen isotope acid digestion fractionation predicted by our cluster model as the ratio of predicted oxygen isotope fractionation between 80 °C and 25 °C, and compare them with the experimental observations (Fig. 8b). The model prediction and experimental data fall close to 1:1 correlation, indicating our cluster model, despite its obvious failure at matching the absolute magnitudes of acid digestion fractionations, captures the variations of the temperature sensitivity of oxygen isotope acid digestion fractionation among different carbonate minerals (including $PbCO_3$; Fig. 8b).

We conclude that our cluster model captures some essential features of the cation effects during phosphoric acid digestion, but is quantitatively inaccurate because it fails to describe the structural relationship between H_2CO_3 and the crystal surface. This deficiency is likely due to the small size and simple geometry of the clusters we have modeled. It should be possible to refine this model so that it simultaneously describes the absolute

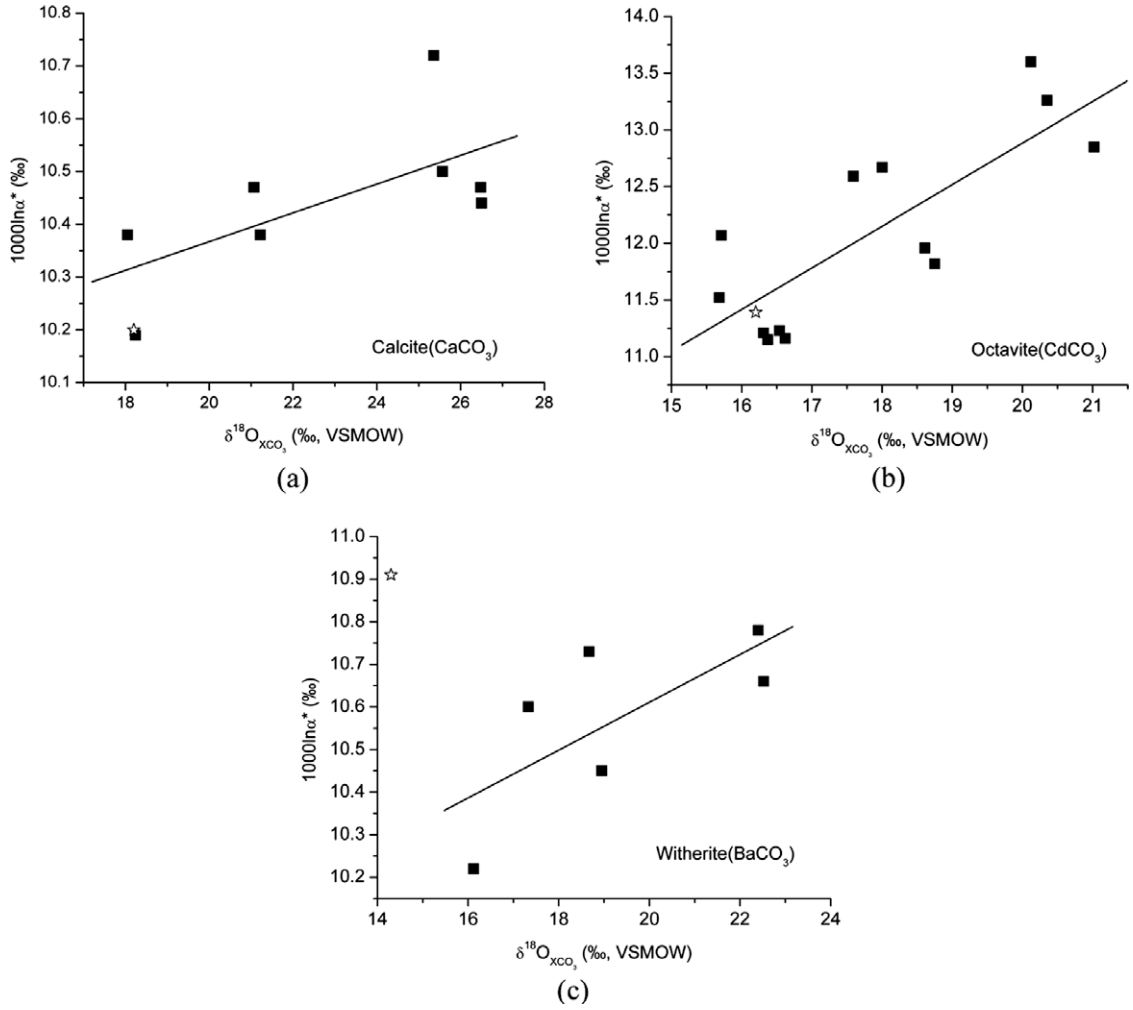

Fig. 7. Empirically observed correlations between the oxygen isotope fractionations associated with phosphoric acid digestion and the oxygen isotopic composition of reactant carbonates. Experimental data are from Kim and O'Neil (1997) and the solid lines are the least square regressions to the experimental data. Neither our H_2CO_3 dissociation model nor our more complex 'cluster' models predict a correlation between these two variables. Also shown for comparison (star symbols) are the data from Sharma and Clayton (1965).

values and temperature dependencies of the acid digestion fractionations and their dependence on reactant composition and structure, although we suspect this would require a sophisticated treatment of the extended structures of surfaces that is beyond the scope of this study (e.g., Kerisit et al., 2003). Nevertheless, the fact our cluster model reproduces the observed variations in size and temperature sensitivity of oxygen isotope fractionations among several carbonate minerals, combined with the substantial success of our simpler H_2CO_3-dissociation model in describing the systematics of phosphoric acid fractionations generally, suggests that the conceptual framework will provide a useful foundation for a more structurally complex model of this kind.

4.4.2. Controls on the variations of acid digestion isotope fractionations among different carbonate minerals

Previous attempts (e.g., Bottcher, 1996; Gilg et al., 2003) to understand the variations of acid digestion fractionation among different carbonate minerals examined empirical correlations between the intercept in a plot of $1000\ln\alpha^*$ vs. $1/T^2$ and the radius or mass of the cation in the reactant carbonate (following the suggestion of Sharma and Sharma, 1969b). These efforts failed to reveal any simple correlation shared by all minerals. (Note that, O'Neil, 1986 made an alternate suggestion that $1000\ln\alpha^*$ values for phosphoric acid digestion reactions might also be controlled by reaction rate; Kim and O'Neil, 1997) However, it is not clear what physiochemical meaning should be attached to the intercept in a plot of acid digestion fractionation vs. $1/T^2$. In this study, we focus on the differences of $1000\ln\alpha^*$ among different carbonate minerals at a given temperature (e.g. 25 °C) and its temperature dependencies separately.

We compare values of $1000\ln\alpha^*$ at 25 °C and the temperature dependencies of $1000\ln\alpha^*$ (from both model prediction and experimental determination) for different carbonate minerals against their respective cation radius (Fig. 9). The theoretically predicted values of $1000\ln\alpha^*$ at 25 °C positively

Table 5
Dependences of phosphoric acid digestion fractionations on the isotopic compositions and the distributions of multiply-substituted isotopologues in reactant carbonates at 25 °C.

CO_3^{2-} in reactant carbonate	$\delta^{13}C_{VPDB}$(‰)	0	10	0	0	10	0	0	10	0
	$\delta^{18}O_{VSMOW}$(‰)	0	0	10	0	0	10	0	0	10
	Equil. T[a] (K)	Random	Random	Random	500	500	500	300	300	300
	Δ_{63}[a] (‰)	0	0	0	0.101	0.101	0.101	0.382	0.382	0.382
	Δ_{64}[a] (‰)	0	0	0	0.042	0.042	0.042	0.155	0.155	0.155
	Δ_{65}[a] (‰)	0	0	0	0.248	0.248	0.248	0.937	0.937	0.937
Model prediction on product CO_2	$\delta^{18}O_{VSMOW}$ (‰)	10.776	10.776	20.884	10.776	10.776	20.884	10.774	10.774	20.882
	Δ_{47} (‰)	0.220	0.220	0.220	0.324	0.324	0.324	0.615	0.615	0.615
	Δ_{48} (‰)	0.137	0.137	0.137	0.180	0.180	0.180	0.297	0.297	0.297
	Δ_{49} (‰)	0.593	0.593	0.592	0.847	0.847	0.847	1.555	1.555	1.555
Acid digestion fractionation	$1000\ln\alpha^*$ (‰)	10.719	10.719	10.719	10.718	10.718	10.718	10.717	10.717	10. 717
	Δ^*_{47} (‰)	0.220	0.220	0.220	0.223	0.223	0.223	0.233	0.233	0.233
	Δ^*_{48} (‰)	0.137	0.137	0.137	0.138	0.138	0.138	0.142	0.142	0.142
	Δ^*_{49} (‰)	0.593	0.593	0.593	0.660	0.660	0.660	0.618	0.618	0.618

[a] Hypothetical equilibration temperature for the distributions of multiply-substituted isotopologues inside reactant carbonates. Δ_{63}, Δ_{64}, and Δ_{65} (see text for definitions) are estimated based on calculations for an isolated CO_3^{2-} group in the gas phase (see Appendix A-1 for details).

Table 6
Variations of acid digestion isotope fractionations and their temperature dependencies among different carbonate minerals, predicted from our cluster model. The cation radius and mass are shown for comparison.

Carbonate minerals		$MgCO_3$	$ZnCO_3$	$FeCO_3$	$MnCO_3$	$CaCO_3$	$SrCO_3$	$PbCO_3$	$BaCO_3$	$^{40}MgCO_3$	$^{40}BaCO_3$
Cation radius[a] r, (Å)		0.65	0.70	0.79	0.80	1.02 (cal) 1.26 (arag)	1.35	1.41	1.55	0.65	1.55
Cation mass, m		24	65	56	55	40	88	207	137	40	40
25 °C	$1000\ln\alpha^*$	3.4844	3.3885	3.6518	3.3369	3.0630	2.8842	1.7706	3.0994	3.5143	3.0923
	Δ^*_{47}	0.0651	0.0572	0.0474	0.0375	0.0708	0.0725	0.0581	0.0761	0.0648	0.0762
	Δ^*_{48}	−0.0494	−0.0311	−0.0581	−0.0538	−0.0460	−0.0439	−0.0386	−0.0367	−0.0501	−0.0366
	Δ^*_{49}	0.0877	0.0810	0.0427	0.0264	0.1028	0.1083	0.0836	0.1227	0.0864	0.1230
50 °C	$1000\ln\alpha^*$	3.1975	3.0878	3.2966	3.0043	2.8263	2.6674	1.6603	2.8628	3.2209	2.8575
	Δ^*_{47}	0.0577	0.0508	0.0422	0.0337	0.0625	0.0639	0.0514	0.0669	0.0574	0.0669
	Δ^*_{48}	−0.0390	−0.0233	−0.0450	−0.0414	−0.0367	−0.0352	−0.0309	−0.0295	−0.0394	−0.0294
	Δ^*_{49}	0.0824	0.0762	0.0446	0.0304	0.0944	0.0988	0.0771	0.1105	0.0815	0.1108
80 °C	$1000\ln\alpha^*$	2.9007	2.7821	2.9404	2.6726	2.5792	2.4400	1.5416	2.6150	2.9185	2.6110
	Δ^*_{47}	0.0499	0.0440	0.0367	0.0295	0.0538	0.0549	0.0443	0.0573	0.0497	0.0574
	Δ^*_{48}	−0.0297	−0.0166	−0.0337	−0.0308	−0.0285	−0.0274	−0.0239	−0.0230	−0.0300	−0.0229
	Δ^*_{49}	0.0751	0.0694	0.0439	0.0319	0.0843	0.0876	0.0691	0.0970	0.0744	0.0971

[a] Cation radii from Golyshev et al. (1981). For $CaCO_3$, the Ca cation radii are different in its two polymorphs, calcite and aragonite, and are 1.02 Å and 1.26Å respectively.

correlate with the reciprocal of cation radius (Fig. 9a). The theoretically predicted, as opposed to experimentally determined, $1000\ln\alpha^*$ at 25 °C show better correlations in this comparison, because significant uncertainties are associated with experimental determinations of $1000\ln\alpha^*$ (more specifically, associated with the determination of total oxygen isotopic compositions of reactant carbonates through the fluorination methods; Kim et al., 2007). In contrast, both theoretically predicted and the experimentally determined temperature dependencies of $1000\ln\alpha^*$ exhibit positive correlations with the reciprocal of cation radius (Fig. 9c and d). The experimental determinations of the temperature dependencies of the oxygen isotope acid fractionation have much smaller uncertainties (since the uncertainties associated with fluorination methods cancel out in the determination of temperature dependence), and therefore show better correlation in the above comparison. The existence of these correlations suggests that cation radius is the most important mineral-specific factor controlling acid digestion fractionations.

To examine the possible effects of cation mass on the acid digestion fractionation, we adopt a similar strategy to that employed by Schauble et al. (2006) in their discussion of equilibrium carbon and oxygen isotope fractionations among different carbonate minerals, and create two hypothetical isotopic carbonates, $^{40}MgCO_3$ and $^{40}BaCO_3$. In these cluster models, all the optimization and calculation were performed in the same manner as outlined

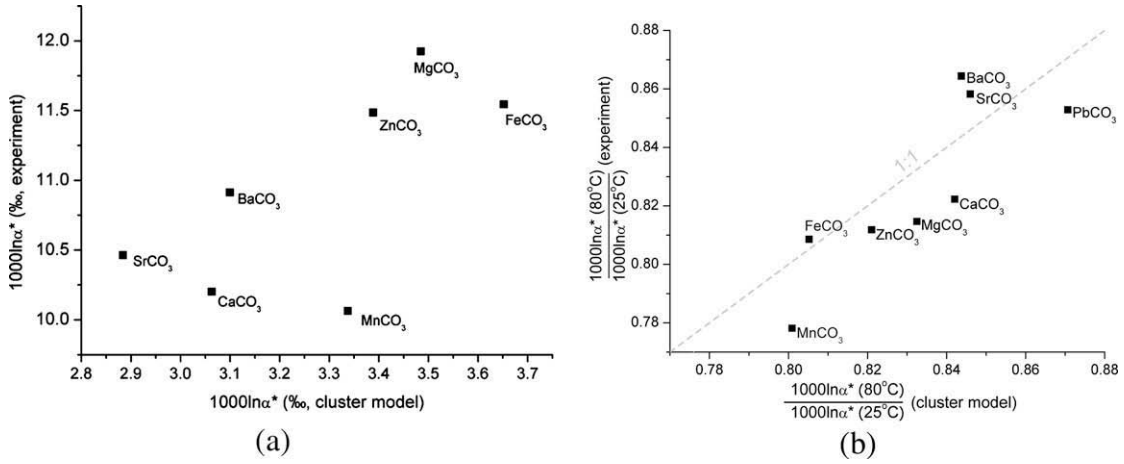

Fig. 8. Comparison of the isotope fractionations associated with phosphoric acid digestion predicted by our 'cluster models' with experimentally observed fractionations for various metal carbonates. Panel (a) depicts the oxygen isotope fractionation at 25 °C; (b) depicts the temperature sensitivity of the oxygen isotope fractionation, as measured by the ratio of oxygen isotope fractionations at 80 °C and 25 °C. Experimental data were based on equations in Table 4. The dashed line in panel (b) indicates a 1:1 correlation.

above for their isotopically normal equivalents, except the atomic masses of Mg and Ba were both assigned as 40 amu instead of their normal masses (24.3 amu and 137.3 amu, respectively). If cation mass controls the acid digestion fractionation, we would expect the model predicted fractionation for these two hypothetical carbonates to closely resemble the predicted fractionation for $CaCO_3$, which has a cation mass of 40.1 amu. Instead, we observe negligible differences in predicted acid digestion fractionations between these hypothetical carbonates and their isotopically normal equivalents (within 0.03‰ for $MgCO_3$ and 0.01‰ for $BaCO_3$; Table 6). Thus, the cation effect on acid digestion fractionation most likely reflects cation size, not mass.

Besides cation radius and mass, crystal structure has been invoked by previous studies as another potential factor that might place important controls on the acid digestion fractionation (Gilg et al., 2003). The fact that our cluster model, which did not consider the effects of crystal structure, managed to semi-quantitatively reproduce the general trend of variations of acid digestion fractionations among different carbonate minerals (Fig. 8), suggests that the crystal structure, like cation mass, exerts only very weak control on the acid digestion fractionation.

4.4.3. Cluster model results on the fractionation of ^{13}C–^{18}O doubly substituted isotopologues during phosphoric acid digestion

Our cluster model predicts that the Δ_{47}^* values associated with phosphoric acid digestion at 25 °C range from 0.0375‰ ($MnCO_3$) to 0.0761‰ ($BaCO_3$) among the eight carbonates mineral studied (Table 6). As for oxygen isotope acid digestion fractionations, our cluster model appears to underestimate the absolute values of Δ_{47}^* fractionations associated with phosphoric acid digestion. Most of the predicted values of Δ_{47}^* are approximately 1/3 to 1/4 of experimental observed Δ_{47}^* for calcite (0.23‰, Section 4.1).

We observe that values of Δ_{47}^* predicted by our cluster model correlate negatively with their respective predicted $1000\ln\alpha^*$ fractionations during phosphoric acid digestion (Fig. 10). If this correlation is general to all carbonate minerals, one could predict the Δ_{47}^* during acid digestion of any carbonate mineral, XCO_3 (where X is a cation), at temperature T:

$$\Delta_{47}^*(XCO_3, T) = \frac{1000\ln\alpha^*(H_2CO_3, T)}{1000\ln\alpha^*(XCO_3, T)} \times \Delta_{47}^*(H_2CO_3, T) \quad (17)$$

where $1000\ln\alpha^*(XCO_3, T)$ is the experimentally determined oxygen isotope acid fractionation at temperature T, and $1000\ln\alpha^*(H_2CO_3, T)$ and $\Delta_{47}^*(H_2CO_3, T)$ are the predicted oxygen isotope and Δ_{47}^* acid digestion fractionation at temperature T from our transition-state-theory H_2CO_3 dissociation model. Note, this relationship examines an empirical correlation between two properties that are grossly underpredicted by our cluster model. Nevertheless, the statistical relationship is strong and thus might provide some basis for predicting the currently unknown relationships between cation content and acid digestion fractionations of ^{13}C–^{18}O bonds. At 25 °C, this gives $\Delta_{47}^* = \frac{10.72}{1000\ln\alpha^*(XCO_3, 25\ °C)} \times 0.220$. This relationship predicts that the acid digestion fractionation, Δ_{47}^*, for different carbonates ranges from 0.198‰ ($MgCO_3$) to 0.234‰ ($MnCO_3$) at 25 °C (Table 4). More specifically, it predicts that the acid digestion fractionation, Δ_{47}^*, for calcite is 0.231‰ at 25 °C—in agreement with our experimentally determined value of 0.232 ± 0.015‰.

We combine previous theoretical estimations on the temperature dependence of ^{13}C–^{18}O and ^{18}O–^{17}O clumping in various carbonate minerals (Schauble et al., 2006) with our predicted acid digestion fractionations, Δ_{47}^*, to predict the temperature calibration lines for the clumped isotope thermometer in various carbonates (i.e., Δ_{47} of CO_2 derived from the phosphoric acid digestion v.s. temperature; Fig. 11). Note that, ^{18}O–^{17}O clumping was reported only

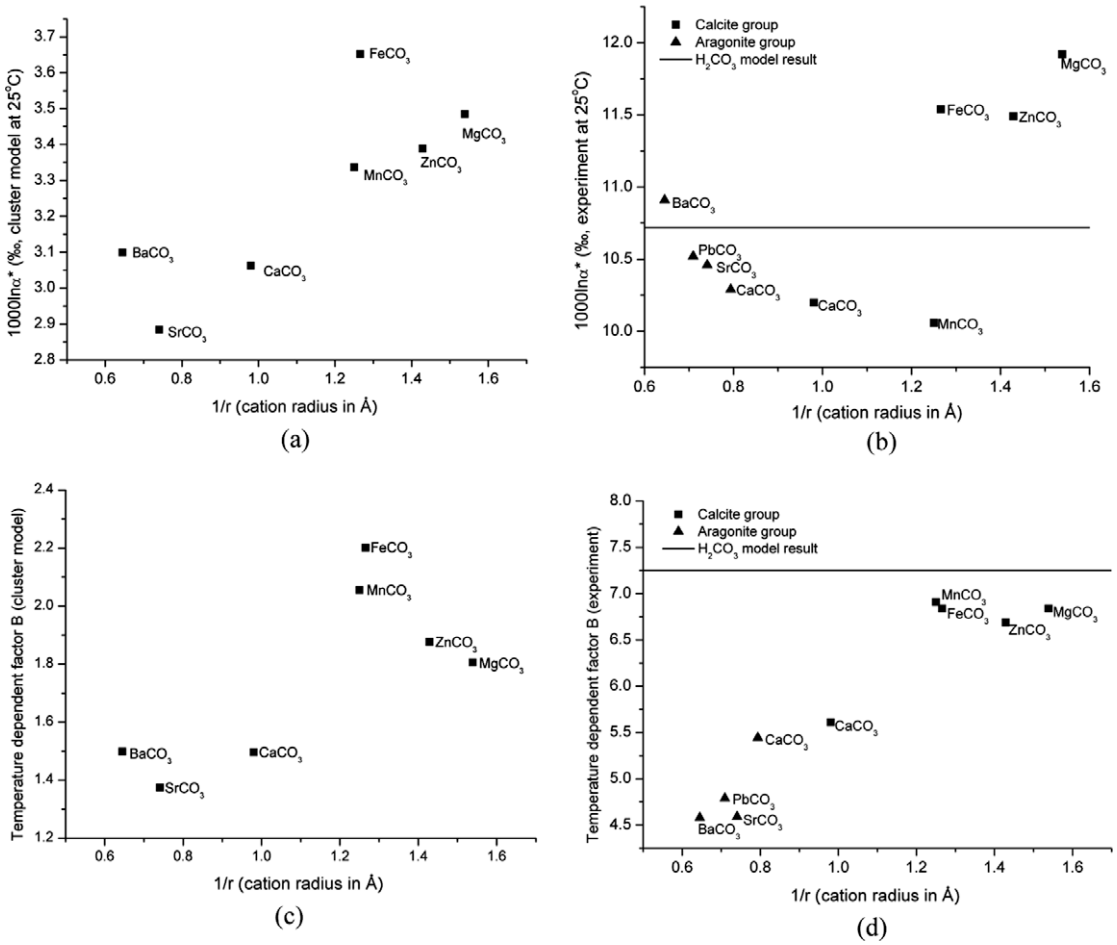

Fig. 9. Correlations between fractionations of oxygen isotopes associated with acid digestion and the ionic radius of the cation in the reactant carbonate. Panel (a) depicts the predicted fractionations of our 'cluster model' for phosphoric acid digestion at 25 °C; (b) experimentally determined acid digestion fractionation at 25 °C; (c) shows 'cluster model' predicted temperature dependence factor B for oxygen isotope acid digestion fractionation (as expressed in the form of $1000\ln\alpha^* = A + B \times 10^5/T^2$; Table 4); (d) experimentally determined temperature dependence factor B for oxygen isotope acid digestion fractionation, against cation radius. These observed correlations indicate cation radius is the predominant factor controlling the variations of acid digestion fractionations among different carbonate minerals. Data on the cation radii are from Golyshev et al. (1981).

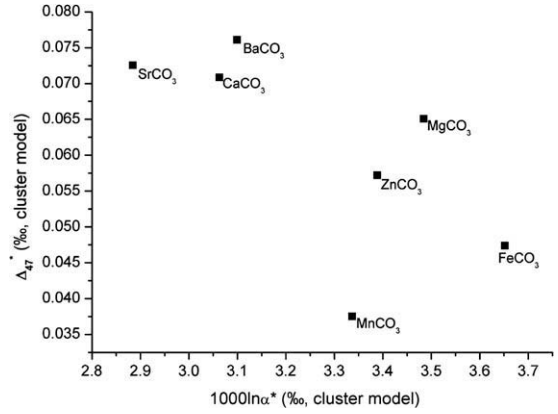

Fig. 10. Inverse correlation between the oxygen isotope fractionation and Δ^*_{47} fractionation during phosphoric acid digestion of different carbonate minerals, predicted from our cluster model.

for calcite in Schauble et al. (2006). We therefore assume in our estimation the same ^{18}O–^{17}O clumping as in calcite for all carbonate minerals. We think this is an appropriate assumption and will not introduce any significant system errors in our estimation, because ^{18}O–^{17}O clumping effects contribute only ~0.7% of Δ_{63} signal in the carbonate minerals and furthermore are suspected to vary negligibly among different carbonate minerals based on the reported variation of ^{13}C–^{18}O clumping effects (less than 7% variations among different carbonate minerals at 25 °C; Schauble et al., 2006). The combination of these two theoretical approaches suggests that the Δ^{47} value of CO_2 extracted at a given temperature from different carbonates minerals grown at the same temperatures can vary by as much as 0.05‰, decreasing in the order: $CaCO_3$(aragonite) > $CaCO_3$ (calcite) > $BaCO_3$(witherite) > $CaMgCO_3$(dolomite) ~ $MgCO_3$ (magnesite). The temperature calibration line predicted in this way for calcite and aragonite closely

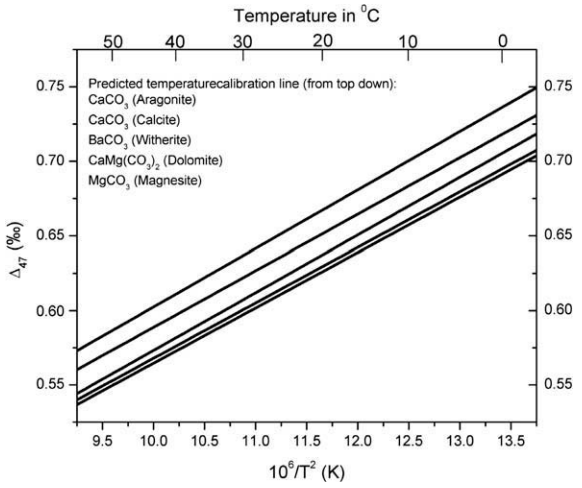

Fig. 11. Predicted temperature calibration lines for different carbonate clumped isotope thermometers, by combining predicted equilibrium ^{13}C–^{18}O and ^{18}O–^{17}O clumping effects inside the carbonate minerals (Schauble et al., 2006) and predicted Δ^*_{47} kinetic fractionations during phosphoric acid digestion of carbonate minerals (this study; see text for details). Phosphoric acid digestions of carbonate minerals are assumed to be at 25 °C.

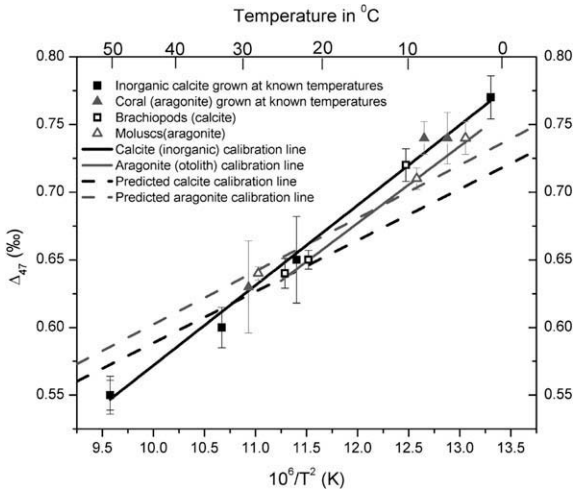

Fig. 12. Comparison between predicted temperature calibration lines for $CaCO_3$ (calcite and aragonite) clumped isotope thermometer (this study) and the experimental temperature calibration data (Ghosh et al., 2006; Ghosh et al., 2007; Came et al., 2007). Phosphoric acid digestions of carbonate minerals are performed at 25 °C.

approach the available experimental calibrations (Ghosh et al., 2006, 2007; Came et al., 2007; Fig 12). However, the slope of our theoretical calibration line is significantly shallower than that of the experimental calibration line at low temperatures (~300 K), with a temperature sensitivity of −0.00289‰/°C over the temperature range 0–50 °C, as compared to the −0.00453‰/°C sensitivity determined experimentally. Finally, for future reference, our predicted calibration line for calcite, dolomite, and magnesite can be represented over the temperature range 260–1500 K by

$$\text{Calcite } \Delta_{47} = -\frac{3.33040\times10^9}{T^4}+\frac{2.32415\times10^7}{T^3} -\frac{2.91282\times10^3}{T^2}-\frac{5.54042}{T}+0.23252 \quad (18)$$

$$\text{Aragonite } \Delta_{47} = -\frac{3.43068\times10^9}{T^4}+\frac{2.35766\times10^7}{T^3} -\frac{8.06003\times10^2}{T^2}-\frac{6.90300}{T}+0.22893 \quad (19)$$

$$\text{Dolomite } \Delta_{47} = -\frac{3.31647\times10^9}{T^4}+\frac{2.29414\times10^7}{T^3} -\frac{2.38375\times10^3}{T^2}-\frac{5.71692}{T}+0.21502 \quad (20)$$

$$\text{Magnesite } \Delta_{47} = -\frac{3.31658\times10^9}{T^4}+\frac{2.19871\times10^7}{T^3} -\frac{2.83346\times10^3}{T^2}-\frac{8.39513}{T}+0.19897 \quad (21)$$

where T is the temperature in Kelvin and phosphoric acid digestions of carbonate minerals are assumed to be at 25 °C.

5. SUMMARY

We present the first quantitative theoretical models of the isotope fractionations during phosphoric acid digestion of carbonate minerals, by using classical transition state theory and ab initio calculations to predict the relative rates of reaction of all the isotopologues of reactant carbonate species. These models assume that the critical reaction intermediate during phosphoric acid digestion is H_2CO_3, and thus that isotope fractionations associated with acid digestion are controlled by kinetic isotope effects during dissociation of H_2CO_3. The simplest form of this model (which considers only H_2CO_3 dissociation as isolated free molecules) predicts the isotope fractionations between product CO_2 and reactant carbonate to be:

$$1000\ln\alpha^* = 2.58 + 7.25\times10^5/T^2, \quad (22)$$

$$\Delta^*_{47} = 0.0242 + 0.189\times10^5/T^2, \quad (23)$$

$$\Delta^*_{48} = -0.0825 + 0.213\times10^5/T^2, \quad (24)$$

$$\Delta^*_{49} = -0.0308 + 0.602\times10^5/T^2, \quad (25)$$

where T is the temperature of acid digestion and in the unit of Kelvin. Both the magnitudes (10.72‰, 0.220‰, 0.137‰, 0.592‰ for $1000\ln\alpha^*, \Delta^*_{47}, \Delta^*_{48}, \Delta^*_{49}$ respectively, at 25 °C) and the temperature-dependences of the these predicted isotope fractionations agree well with available experimental data on oxygen isotope fractionations and our newly determined Δ_{47} fractionation of 0.232 ± 0.015‰ for calcite during phosphoric acid digestion.

A subset of our models attempt to take into account also the influence of cation composition by permitting

the H_2CO_3 reaction intermediate to interact with an adjacent metal carbonate group. These 'cluster models' underestimate the magnitude of isotope fractionations associated with phosphoric acid digestion by a factor of ~3, presumably because we have incorrectly described the structure of nearest-neighbor interactions between H_2CO_3 reaction intermediate and the reacting mineral surface. Nevertheless, our cluster models reproduce the general trend of variations (in both size and temperature sensitivity) of oxygen isotope acid digestion fractionation among different carbonate minerals, which therefore provides a general concept framework for future, more sophisticated first-principles models of the carbonate-acid interface.

ACKNOWLEDGMENTS

We thank Edwin Schauble for helpful discussions on the equilibrium clumped isotope effects in carbonate minerals. We thank Juske Horita for his editorial handling of this manuscript, and two anonymous reviewers for thoughtful and constructive comments.

APPENDIX A

A.1. Estimation on the equilibrium distributions of multiply-substituted isotopologues inside reactant carbonate mineral for assumed temperatures and bulk isotopic compositions

We calculate the distributions of all singly and multiply-substituted isotopologues inside reactant carbonate mineral at assumed equilibration temperatures, following the methodology and algorithms presented by Wang et al. (2004) in their theoretical estimations of abundances of multiply-substituted isotopologues of molecular gases. CO_3^{2-} in a reactant carbonate mineral has a total of 20 isotopologues. To determine the abundances of all isotopologues, we select the abundances of non-substituted ($^{12}C^{16}O^{16}O^{16}O^{2-}$) and singly-substituted isotopologues ($^{13}C^{16}O^{16}O^{16}O^{2-}$, $^{12}C^{18}O^{16}O^{16}O^{2-}$ and $^{12}C^{17}O^{16}O^{16}O^{2-}$) as the fundamental unknowns, and express the abundances of the other 16 multiply-substituted isotopologues as functions of these fundamental unknowns and the equilibrium constants of the related isotope exchange reactions:

$$[^{13}C^{18}O^{16}O^{16}O^{2-}] = \frac{[^{13}C^{16}O^{16}O^{16}O^{2-}] \times [^{12}C^{18}O^{16}O^{16}O^{2-}]}{[^{12}C^{16}O^{16}O^{16}O^{2-}]} \times K_{3866} \quad (a1)$$

$$[^{13}C^{17}O^{16}O^{16}O^{2-}] = \frac{[^{13}C^{16}O^{16}O^{16}O^{2-}] \times [^{12}C^{17}O^{16}O^{16}O^{2-}]}{[^{12}C^{16}O^{16}O^{16}O^{2-}]} \times K_{3766} \quad (a2)$$

$$[^{12}C^{17}O^{17}O^{16}O^{2-}] = \frac{[^{12}C^{17}O^{16}O^{16}O^{2-}]^2}{[^{12}C^{16}O^{16}O^{16}O^{2-}]} \times K_{2776} \quad (a3)$$

$$[^{12}C^{17}O^{18}O^{16}O^{2-}] = \frac{[^{12}C^{17}O^{16}O^{16}O^{2-}] \times [^{12}C^{18}O^{16}O^{16}O^{2-}]}{[^{12}C^{16}O^{16}O^{16}O^{2-}]} \times K_{2786} \quad (a4)$$

$$[^{13}C^{17}O^{17}O^{16}O^{2-}] = \frac{[^{13}C^{16}O^{16}O^{16}O^{2-}] \times [^{12}C^{17}O^{16}O^{16}O^{2-}]^2}{[^{12}C^{16}O^{16}O^{16}O^{2-}]^2} \times K_{3766} \quad (a5)$$

$$[^{12}C^{17}O^{17}O^{17}O^{2-}] = \frac{[^{12}C^{17}O^{16}O^{16}O^{2-}]^3}{[^{12}C^{16}O^{16}O^{16}O^{2-}]^2} \times K_{2777} \quad (a6)$$

$$[^{12}C^{18}O^{18}O^{16}O^{2-}] = \frac{[^{12}C^{18}O^{16}O^{16}O^{2-}]^2}{[^{12}C^{16}O^{16}O^{16}O^{2-}]} \times K_{2886} \quad (a7)$$

$$[^{13}C^{17}O^{18}O^{16}O^{2-}] = \frac{[^{13}C^{16}O^{16}O^{16}O^{2-}] \times [^{12}C^{17}O^{16}O^{16}O^{2-}] \times [^{12}C^{18}O^{16}O^{16}O^{2-}]}{[^{12}C^{16}O^{16}O^{16}O^{2-}]^2} \times K_{3786} \quad (a8)$$

$$[^{12}C^{17}O^{17}O^{18}O^{2-}] = \frac{[^{12}C^{17}O^{16}O^{16}O^{2-}]^2 \times [^{12}C^{18}O^{16}O^{16}O^{2-}]}{[^{12}C^{16}O^{16}O^{16}O^{2-}]^2} \times K_{2778} \quad (a9)$$

$$[^{13}C^{17}O^{17}O^{17}O^{2-}] = \frac{[^{13}C^{16}O^{16}O^{16}O^{2-}] \times [^{12}C^{17}O^{16}O^{16}O^{2-}]^3}{[^{12}C^{16}O^{16}O^{16}O^{2-}]^3} \times K_{3777} \quad (a10)$$

$$[^{13}C^{18}O^{18}O^{16}O^{2-}] = \frac{[^{13}C^{16}O^{16}O^{16}O^{2-}] \times [^{12}C^{18}O^{16}O^{16}O^{2-}]^2}{[^{12}C^{16}O^{16}O^{16}O^{2-}]^2} \times K_{3886} \quad (a11)$$

$$[^{12}C^{17}O^{18}O^{18}O^{2-}] = \frac{[^{12}C^{17}O^{16}O^{16}O^{2-}] \times [^{12}C^{18}O^{16}O^{16}O^{2-}]^2}{[^{12}C^{16}O^{16}O^{16}O^{2-}]^2} \times K_{2788} \quad (a12)$$

$$[^{13}C^{17}O^{18}O^{18}O^{2-}] = \frac{[^{13}C^{16}O^{16}O^{16}O^{2-}] \times [^{12}C^{17}O^{16}O^{16}O^{2-}] \times [^{12}C^{18}O^{16}O^{16}O^{2-}]^2}{[^{12}C^{16}O^{16}O^{16}O^{2-}]^3} \times K_{3788} \quad (a13)$$

$$[^{12}C^{18}O^{18}O^{18}O^{2-}] = \frac{[^{12}C^{18}O^{16}O^{16}O^{2-}]^3}{[^{12}C^{16}O^{16}O^{16}O^{2-}]^2} \times K_{2888} \quad (a14)$$

$$[^{13}C^{17}O^{18}O^{18}O^{2-}] = \frac{[^{13}C^{16}O^{16}O^{16}O^{2-}] \times [^{12}C^{17}O^{16}O^{16}O^{2-}] \times [^{12}C^{18}O^{16}O^{16}O^{2-}]^2}{[^{12}C^{16}O^{16}O^{16}O^{2-}]^3} \times K_{3788} \quad (a15)$$

$$[^{13}C^{18}O^{18}O^{18}O^{2-}] = \frac{[^{13}C^{16}O^{16}O^{16}O^{2-}] \times [^{12}C^{18}O^{16}O^{16}O^{2-}]^3}{[^{12}C^{16}O^{16}O^{16}O^{2-}]^3} \times K_{3888} \quad (a16)$$

where K denote the equilibrium constants for the related isotope exchange reactions at the specified equilibration temperature, e.g.,

$$^{13}C^{16}O^{16}O^{16}O^{2-} + {}^{12}C^{18}O^{16}O^{16}O^{2-} \longleftrightarrow {}^{13}C^{18}O^{16}O^{16}O^{2-} + {}^{12}C^{16}O^{16}O^{16}O^{2-}$$

$$K_{3866} = \frac{Q_{^{13}C^{18}O^{16}O^{16}O^{2-}} \times Q_{^{12}C^{16}O^{16}O^{16}O^{2-}}}{Q_{^{13}C^{16}O^{16}O^{16}O^{2-}} \times Q_{^{12}C^{18}O^{16}O^{16}O^{2-}}}$$

$$^{13}C^{16}O^{16}O^{16}O^{2-} + {}^{12}C^{17}O^{16}O^{16}O^{2-} + {}^{12}C^{18}O^{16}O^{16}O^{2-} \longleftrightarrow {}^{13}C^{17}O^{18}O^{16}O^{2-} + 2 \times {}^{12}C^{16}O^{16}O^{16}O^{2-}$$

$$K_{3786} = \frac{Q_{^{13}C^{17}O^{18}O^{16}O^{2-}} \times (Q_{^{12}C^{16}O^{16}O^{16}O^{2-}})^2}{Q_{^{13}C^{16}O^{16}O^{16}O^{2-}} \times Q_{^{12}C^{17}O^{16}O^{16}O^{2-}} \times Q_{^{12}C^{18}O^{16}O^{16}O^{2-}}}$$

Q here refer to the partition functions of different CO_3^{2-} isotopologues, and can be evaluated with their respective scaled vibration frequencies through principles of statistical thermodynamics (Urey 1947).

Rather than performing complete calculations of these 16 equilibrium constants for multiply-substituted isotopologues in carbonate mineral lattices, as Schauble et al. (2006) did for K_{3866} and K_{2876}, we reduced the necessary computation power by calculating the corresponding equilibrium constants for isolated CO_3^{2-} ions in the gas phase, and use them to approximate the equilibrium constants in carbonate lattice. The distribution of multiply-substituted isotopologues inside the two are remarkably similar (e.g., at equilibration temperature of 300 K, $K_{3866} = 1.0004034$ in isolated CO_3^{2-}, this study; v.s. $K_{3866} = 1.0004066$ in calcite lattice, Schauble et al., 2006), and therefore this approximation appears not to introduce any significant systematic errors on our model results. The geometry optimization and frequency calculation for the isolated CO_3^{2-} ion are performed at DFT-B3LYP/6-31G* level, and the frequencies are scaled with the universal scaling factor of 0.9614 as discussed in Section 2.3 (Table A1).

We combine the above equations with the constraints from the bulk isotopic composition of the CO_3^{2-} ion,

$$[^{13}C^{16}O^{16}O^{16}O^{2-}] + [^{13}C^{17}O^{16}O^{16}O^{2-}] + [^{13}C^{18}O^{16}O^{16}O^{2-}] + [^{13}C^{17}O^{17}O^{16}O^{2-}] + [^{13}C^{17}O^{18}O^{16}O^{2-}] + [^{13}C^{18}O^{18}O^{16}O^{2-}] + [^{13}C^{17}O^{17}O^{17}O^{2-}] + [^{13}C^{17}O^{17}O^{18}O^{2-}] + [^{13}C^{17}O^{18}O^{18}O^{2-}] + [^{13}C^{18}O^{18}O^{18}O^{2-}] = [^{13}C] \quad (a17)$$

$$[^{12}C^{18}O^{16}O^{16}O^{2-}] + [^{12}C^{17}O^{18}O^{16}O^{2-}] + [^{12}C^{17}O^{17}O^{18}O^{2-}] + [^{13}C^{18}O^{16}O^{16}O^{2-}] + [^{13}C^{17}O^{18}O^{16}O^{2-}] + [^{13}C^{17}O^{17}O^{18}O^{2-}] + 2 \times [^{12}C^{18}O^{18}O^{16}O^{2-}] + 2 \times [^{12}C^{17}O^{18}O^{18}O2-] + 2 \times [^{13}C^{18}O^{18}O^{16}O^{2-}] + 2 \times [^{13}C^{17}O^{18}O^{18}O^{2-}] + 3 \times [^{12}C^{18}O^{18}O^{18}O^{2-}] + 3 \times [^{13}C^{18}O^{18}O^{18}O^{2-}] = 3 \times [^{18}O] \quad (a18)$$

$$3 \times [^{12}C^{16}O^{16}O^{16}O^{2-}] + 2 \times [^{12}C^{17}O^{16}O^{16}O^{2-}] + 2[^{12}C^{18}O^{16}O^{16}O^{2-} + [^{12}C^{17}O^{17}O^{16}O^{2-}] + [^{12}C^{17}O^{18}O^{16}O^{2-}] + [^{12}C^{18}O^{18}O^{16}O^{2-}] + 3 \times [^{13}C^{16}O^{16}O^{16}O^{2-}] + 2 \times [^{13}C^{17}O^{16}O^{16}O^{2-}] + 2 \times [^{13}C^{18}O^{16}O^{16}O^{2-}] + [^{13}C^{17}O^{17}O^{16}O^{2-}] + [^{13}C^{17}O^{18}O^{16}O^{2-}] + [^{13}C^{18}O^{18}O^{16}O^{2-}] = 3 \times [^{16}O] \quad (a19)$$

$$[^{12}C^{16}O^{16}O^{16}O^{2-}] + [^{12}C^{17}O^{16}O^{16}O^{2-}] + [^{12}C^{18}O^{16}O^{16}O^{2-}] + [^{12}C^{17}O^{17}O^{16}O^{2-}] + [^{12}C^{17}O^{18}O^{16}O^{2-}] + [^{12}C^{18}O^{18}O^{16}O^{2-}] + [^{12}C^{17}O^{17}O^{17}O^{2-}] + [^{12}C^{17}O^{17}O^{18}O^{2-}] + [^{12}C^{17}O^{18}O^{18}O^{2-}] + [^{12}C^{18}O^{18}O^{18}O^{2-}] + [^{13}C^{16}O^{16}O^{16}O^{2-}] + [^{13}C^{17}O^{16}O^{16}O^{2-}] + [^{13}C^{18}O^{16}O^{16}O^{2-}] + [^{13}C^{17}O^{17}O^{16}O^{2-}] + [^{13}C^{17}O^{18}O^{16}O^{2-}] + [^{13}C^{18}O^{18}O^{16}O^{2-}] + [^{13}C^{17}O^{17}O^{17}O^{2-}] + [^{13}C^{17}O^{17}O^{18}O^{2-}] + [^{13}C^{17}O^{18}O^{18}O^{2-}] + [^{13}C^{18}O^{18}O^{18}O^{2-}] = 1 \quad (a20)$$

where $[^{13}C]$, $[^{18}O]$, $[^{16}O]$ refer to the bulk ^{13}C, ^{18}O and ^{16}O abundances in the CO_3^{2-} respectively an can be calculated from its given bulk isotopic composition. By simultaneously solving these 20 equations (using fsolve function in MATLAB program, version 7.04), we obtain the abundances of all 20 isotopologues at specified bulk isotopic composition and equilibration temperature (Table A2).

A.2. Predicted dependence of the fractionations of multiply-substituted isotopologues on proportions of multiply substituted isotopologues of reactant carbonates

Our H_2CO_3 dissociation model predicted an unexpected dependence of the fractionations of multiply-substituted isotopologues (i.e., values of $\Delta^*_{47}, \Delta^*_{48}$ and Δ^*_{49}) on proportions of multiply substituted isotopologues of reactant carbonates (i.e., values of Δ_{63}, Δ_{64}, and Δ_{65}) (Table 5; Section 4.3). We show below this dependence arise from a peculiarity in the way the Δ_i values are defined.

The Δ^*_i values for any particular isotopologue is independent of reactant composition; that is, $\Delta_{^{13}C^{18}O^{16}O}$ of product CO_2 differs from $\Delta_{^{13}C^{18}O^{16}O2}$ of reactant carbonate by an amount that varies with temperature but is independent of the $\Delta_{^{13}C^{18}O^{16}O^{16}O}$ of reactant carbonate. However, for the fractionation of total mass 47 isotopologues,

$$\begin{aligned}\Delta^*_{47} &= \Delta_{47} - \Delta_{63} \\ &\approx \left(f_{^{13}C^{18}O^{16}O} \times \Delta_{^{13}C^{18}O^{16}O} + f_{^{12}C^{18}O^{17}O} \times \Delta_{^{12}C^{18}O^{17}O} + f_{^{13}C^{17}O_2} \times \Delta_{^{13}C^{17}O_2}\right) - \left(f_{^{13}C^{18}O^{16}O_2} \times \Delta_{^{13}C^{18}O^{16}O_2} + f_{^{12}C^{18}O^{17}O^{16}O} \times \Delta_{^{12}C^{18}O^{17}O^{16}O} + f_{^{13}C^{16}O^{17}O_2} \times \Delta_{^{13}C^{16}O^{17}O_2} + f_{^{12}C^{17}O_3} \times \Delta_{^{12}C^{17}O_3}\right)\end{aligned}$$

where $f_{^{13}C^{18}O^{16}O}, f_{^{12}C^{18}O^{17}O}, f_{^{13}C^{17}O_2}$ are the relative abundance fractions of isotopologues $^{13}C^{18}O^{16}O$, $^{12}C^{18}O^{17}O$ and $^{13}C^{17}O^{17}O$ in all the mass 47 isotopologues of product CO_2, $f_{^{13}C^{18}O^{16}O_2}, f_{^{12}C^{18}O^{17}O^{16}O}, f_{^{13}C^{16}O^{17}O_2}, f_{^{12}C^{17}O_3}$ are the relative abundance fractions of isotopologues $^{13}C^{18}O^{16}\ O_2^{2-}$, $^{12}C^{18}O^{17}\ O^{16}O$, $^{13}C^{16}\ O^{17}O_2^{2-}$ and $^{12}C^{17}\ O_3^{2-}$ in all the mass 63 isotopologues of reactant carbonate CO_3^{2-}.

Table A1
Scaled vibration frequencies (unit: cm^{-1}) for different CO_3^{2-} isotopologues (isolated CO_3^{2-} in the gas phase, DFT-B3LYP/6-31G* with a frequency scaling factor of 0.9614).

Isotopologue	ϖ_1	ϖ_2	ϖ_3	ϖ_4	ϖ_5	ϖ_6
$^{12}C^{16}O^{16}O^{16}O^{2-}$	638.23	638.23	837.82	975.97	1396.24	1396.24
$^{12}C^{17}O^{16}O^{16}O^{2-}$	631.11	633.21	836.17	966.25	1389.37	1396.21
$^{12}C^{18}O^{16}O^{16}O^{2-}$	624.53	628.54	834.70	957.47	1383.83	1395.88
$^{12}C^{17}O^{17}O^{16}O^{2-}$	625.24	627.02	834.52	956.49	1385.68	1392.85
$^{12}C^{17}O^{18}O^{16}O^{2-}$	618.74	622.36	833.05	947.66	1380.84	1391.67
$^{12}C^{18}O^{18}O^{16}O^{2-}$	612.66	617.32	831.58	938.83	1376.69	1389.69
$^{12}C^{17}O^{17}O^{17}O^{2-}$	620.13	620.13	832.86	946.71	1385.66	1385.66
$^{12}C^{17}O^{17}O^{18}O^{2-}$	612.81	616.30	831.39	937.86	1380.24	1384.94
$^{12}C^{17}O^{18}O^{18}O^{2-}$	607.32	610.76	829.91	928.96	1376.98	1381.94
$^{12}C^{18}O^{18}O^{18}O^{2-}$	603.55	603.55	828.44	920.03	1376.28	1376.28
$^{13}C^{16}O^{16}O^{16}O^{2-}$	636.73	636.73	811.56	975.97	1355.65	1355.65
$^{13}C^{17}O^{16}O^{16}O^{2-}$	629.55	631.86	809.86	966.22	1348.54	1355.62
$^{13}C^{18}O^{16}O^{16}O^{2-}$	622.91	627.33	808.34	957.36	1342.81	1355.30
$^{13}C^{17}O^{17}O^{16}O^{2-}$	623.72	625.72	808.15	956.46	1344.69	1352.15
$^{13}C^{17}O^{18}O^{16}O^{2-}$	617.19	621.16	806.63	947.59	1339.67	1350.95
$^{13}C^{18}O^{18}O^{16}O^{2-}$	611.13	616.17	805.11	938.73	1335.35	1348.93
$^{13}C^{17}O^{17}O^{17}O^{2-}$	618.75	618.75	806.44	946.71	1344.67	1344.67
$^{13}C^{17}O^{17}O^{18}O^{2-}$	611.38	615.06	804.92	937.84	1339.01	1343.97
$^{13}C^{17}O^{18}O^{18}O^{2-}$	605.94	609.54	803.40	928.94	1335.62	1340.86
$^{13}C^{18}O^{18}O^{18}O^{2-}$	602.28	602.28	801.87	920.03	1334.94	1334.94

Table A2
Estimated abundances of all CO_3^{2-} isotopologues at different equilibration temperatures and with different bulk isotopic compositions.

Isotopologue of CO_3^{2-} Reactant	Mass[a]	$\delta^{13}C_{VPDB}$(‰) $\delta^{18}O_{VSMOW}$(‰) Equil. T (K)	0 0 500	10 0 500	0 10 500	0 0 300	10 0 300	0 10 300
$^{12}C^{16}O^{16}O^{16}O^{2-}$	60		0.981845501	0.981736407	0.981780829	0.981845495	0.981736401	0.981780823
$^{13}C^{16}O^{16}O^{16}O^{2-}$	61		0.011033192	0.011142286	0.011032465	0.011033186	0.011142280	0.011032460
$^{12}C^{17}O^{16}O^{16}O^{2-}$	61		0.001119007	0.001118883	0.001124698	0.001119001	0.001118877	0.001124692
$^{12}C^{18}O^{16}O^{16}O^{2-}$	62		0.005906388	0.005905731	0.005965059	0.005906382	0.005905726	0.005965053
$^{13}C^{17}O^{16}O^{16}O^{2-}$	62		1.257521E−05	1.269955E−05	1.263916E−05	1.257710E−05	1.270146E−05	1.264106E−05
$^{12}C^{17}O^{17}O^{16}O^{2-}$	62		6.637827E−05	6.703460E−05	6.703764E−05	6.639792E−05	6.705445E−05	6.705748E−05
$^{13}C^{18}O^{16}O^{16}O^{2-}$	63		4.487818E−06	4.487320E−06	4.555747E−06	4.488118E−06	4.487619E−06	4.556051E−06
$^{12}C^{18}O^{17}O^{16}O^{2-}$	63		4.251179E−07	4.250706E−07	4.294809E−07	4.251298E−07	4.250826E−07	4.294930E−07
$^{13}C^{17}O^{17}O^{16}O^{2-}$	63		1.184398E−05	1.184267E−05	1.208125E−05	1.184530E−05	1.184399E−05	1.208260E−05
$^{12}C^{17}O^{17}O^{17}O^{2-}$	63		5.043864E−08	5.093736E−08	5.120209E−08	5.046478E−08	5.096376E−08	5.122862E−08
$^{12}C^{18}O^{18}O^{16}O^{2-}$	64		4.777666E−09	4.824907E−09	4.826700E−09	4.779286E−09	4.826542E−09	4.828336E−09
$^{13}C^{18}O^{17}O^{16}O^{2-}$	64		1.331213E−07	1.344375E−07	1.357881E−07	1.332149E−07	1.345321E−07	1.358836E−07
$^{12}C^{18}O^{17}O^{17}O^{2-}$	64		5.383609E−11	5.383010E−11	5.466880E−11	5.384187E−11	5.383588E−11	5.467467E−11
$^{13}C^{17}O^{17}O^{17}O^{2-}$	64		8.525078E−10	8.524131E−10	8.698698E−10	8.526678E−10	8.525730E−10	8.700330E−10
$^{13}C^{18}O^{18}O^{16}O^{2-}$	65		4.499842E−09	4.499342E−09	4.613632E−09	4.501037E−09	4.500536E−09	4.614857E−09
$^{12}C^{18}O^{18}O^{17}O^{2-}$	65		7.917198E−09	7.916318E−09	8.156559E−09	7.919962E−09	7.919082E−09	8.159407E−09
$^{13}C^{18}O^{17}O^{17}O^{2-}$	65		6.050678E−13	6.110505E−13	6.144267E−13	6.054144E−13	6.114005E−13	6.147787E−13
$^{12}C^{18}O^{18}O^{18}O^{2-}$	66		9.581874E−12	9.676617E−12	9.777016E−12	9.589474E−12	9.684291E−12	9.784770E−12
$^{13}C^{18}O^{18}O^{17}O^{2-}$	66		5.057908E−11	5.107919E−11	5.185810E−11	5.063019E−11	5.113081E−11	5.191051E−11
$^{13}C^{18}O^{18}O^{18}O^{2-}$	67		8.899522E−11	8.987519E−11	9.168583E−11	8.910502E−11	8.998607E−11	9.179895E−11

[a] Nominal cardinal mass in amu.

We define

$$\Delta^*_{^{13}C^{18}O^{16}O} = \Delta_{^{13}C^{18}O^{16}O} - \Delta_{^{13}C^{18}O^{16}O_2};$$

$$\Delta^*_{^{12}C^{18}O^{17}O} = \Delta_{^{12}C^{18}O^{17}O} - \Delta_{^{12}C^{18}O^{17}O^{16}O};$$

$$\Delta^*_{^{13}C^{17}O_2} = \Delta_{^{13}C^{17}O_2} - \Delta_{^{13}C^{16}O^{17}O_2}$$

as the fractionations of specific isotopologue during phosphoric acid digestion. Substituting these definitions in the equation above, we obtain

$$\begin{aligned}\Delta^*_{47} \approx {} & \left(f_{^{13}C^{18}O^{16}O} \times \Delta^*_{^{13}C^{18}O^{16}O} + f_{^{12}C^{18}O^{17}O} \times \Delta^*_{^{12}C^{18}O^{17}O} \right. \\ & \left. + f_{^{13}C^{17}O_2} \times \Delta^*_{^{13}C^{17}O_2}\right) + \left(f_{^{13}C^{18}O^{16}O} - f_{^{13}C^{18}O^{16}O_2}\right) \\ & \times \Delta_{^{13}C^{18}O^{16}O_2} + \left(f_{^{12}C^{18}O^{17}O} - f_{^{12}C^{18}O^{17}O^{16}O}\right) \\ & \times \Delta_{^{12}C^{18}O^{17}O^{16}O} + \left(f_{^{13}C^{17}O_2} - f_{^{13}C^{16}O^{17}O_2}\right) \times \Delta_{^{13}C^{16}O^{17}O_2} \\ & - f_{^{12}C^{17}O_3} \times \Delta_{^{12}C^{17}O_3}\end{aligned}$$

In carbonates of natural isotopic compositions, $\left(f_{^{13}C^{18}O^{16}O} - f_{^{13}C^{18}O^{16}O_2}\right) \approx -\left(f_{^{12}C^{18}O^{17}O} - f_{^{12}C^{18}O^{17}O^{16}O}\right) \gg -\left(f_{^{13}C^{17}O_2} - f_{^{13}C^{16}O^{17}O_2}\right) \gg f_{^{12}C^{17}O_3}$ and $\Delta_{^{13}C^{18}O^{16}O_2} \gg \Delta_{^{12}C^{18}O^{17}O^{16}O}$ (e.g. for calcite $\Delta_{^{13}C^{18}O^{16}O_2} = 0.406‰$ and $\Delta_{^{12}C^{18}O^{17}O^{16}O} = 0.071‰$ at 300 K; Schauble et al., 2006), the above equation can therefore be further approximated as

$$\Delta^*_{47} \approx \left(f_{^{13}C^{18}O^{16}O} \times \Delta^*_{^{13}C^{18}O^{16}O} + f_{^{12}C^{18}O^{17}O} \times \Delta^*_{^{12}C^{18}O^{17}O} + f_{^{13}C^{17}O_2} \times \Delta^*_{^{13}C^{17}O_2}\right) + \left(f_{^{13}C^{18}O^{16}O} - f_{^{13}C^{18}O^{16}O_2}\right) \times \Delta_{^{13}C^{18}O^{16}O_2}$$

As mentioned above, the Δ^*_i values are independent of Δ_i of the reactant carbonate and are a function of only acid digestion temperature, and thus can be regarded as constant at given temperature (at 25 °C, $\Delta^*_{^{13}C^{18}O^{16}O} = 0.225‰$, $\Delta^*_{^{12}C^{18}O^{17}O} = 0.070‰$ and $\Delta^*_{^{13}C^{17}O^{17}O} = 0.277‰$, respectively):

$$\Delta^*_{47} \approx \text{constant} + \left(f_{^{13}C^{18}O^{16}O} - f_{^{13}C^{18}O^{16}O_2}\right) \times \Delta_{^{13}C^{18}O^{16}O_2} \approx \text{constant} + \left(f_{^{13}C^{18}O^{16}O} - f_{^{13}C^{18}O^{16}O_2}\right) \times \Delta_{63}$$

For carbonates with $\delta^{13}C = 0‰$ and $\delta^{18}O = 0‰$, as assumed in our model, $f_{^{13}C^{18}O^{16}O_2} = 0.9671$ and $f_{^{13}C^{18}O^{16}O} = 0.9366$. Therefore, we expect the dependence of Δ^*_{47} on Δ_{63} of the reactant carbonate to have a slope of ~0.0305, based on the above analyses. This agrees well with our quantitative H_2CO_3 model prediction, ~0.035‰ increase in Δ^*_{47} for every 1‰ increase in Δ_{63}. The small discrepancy is believed to arise from the approximations adopted in the derivation of the above equations. Note that this slope for the dependence of Δ^*_{47} on Δ_{63} varies little for carbonates of different bulk isotopic compositions, since both $f_{^{13}C^{18}O^{16}O}$ and $f_{^{13}C^{18}O^{16}O_2}$ are insensitive to the changes in the bulk isotopic compositions. The slope increases by only ~0.002 for 50‰ increase in $\delta^{13}C$, and decrease by ~0.0005 for 50‰ increase in $\delta^{18}O$.

REFERENCES

Al-Hosney H. A. and Grassian V. H. (2004) Carbonic acid: an important intermediate in the surface chemistry of calcium carbonate. *J. Amer. Chem. Soc.* **126**, 8068–8069.

Al-Hosney H. A. and Grassian V. H. (2005) Water, sulfur dioxide and nitric acid adsorption on calcium carbonate: a transmission and ATR-FTIR study. *Phys. Chem. Chem. Phys.* **7**, 1266–1276.

Assonov S. S. and Brenninkmeijer C. A. M. (2003) On the ^{17}O correction for CO_2 mass spectrometric isotopic analysis. *Rapid Commun. Mass Spectrom.* **17**, 1007–1016.

Barkan E. and Luz B. (2005) High precision measurements of $^{17}O/^{16}O$ and $^{18}O/^{16}O$ ratios in H_2O. *Rapid Commun. Mass Spectrom.* **19**, 3737–3742.

Bottcher M. (1996) $^{18}O/^{16}O$ and $^{13}C/^{12}C$ fractionation during the reaction of carbonates with phosphoric acid: effects of cationic substitution and reaction temperature. *Isot. Environ. Health Stud.* **32**, 299–305.

Came R. E., Eiler J. M., Veizer J., Azmy K., Brand U. and Weidman C. R. (2007) Coupling of surface temperatures and atmospheric CO_2 concentrations during the Palaeozoic era. *Nature* **449**, 198–201.

Coplen T. B., Kendall C. and Hopple J. (1983) Comparison of stable isotope reference samples. *Nature* **302**, 236–238.

Das Sharma S., Patil D. J. and Gopalan K. (2002) Temperature dependence of oxygen isotope fractionation of CO_2 from magnesite-phosphoric acid reaction. *Geochim. Cosmochim. Acta* **66**, 589–593.

Des Marais D. J. (1997) Long-term evolution of the biogeochemical carbon cycle. *Rev. Miner. Geochem.* **35**, 429–448.

Eiler J. M. and Schauble E. (2004) $^{18}O^{13}C^{16}O$ in Earth's atmosphere. *Geochim. Cosmochim. Acta* **68**, 4767–4777.

Eyring H. (1935a) Activated complex in chemical reactions. *J. Chem. Phys.* **3**, 107–115.

Eyring H. (1935b) The activated complex and the absolute rate of chemical reactions. *Chem. Rev.* **17**, 65–77.

Felipe M. A., Xiao Y. and Kubicki J. D. (2001) Molecular orbital modeling and transition state theory in geochemistry. *Rev. Mineral. Geochem.* **42**, 485–531.

Foresman, J.B., Frisch, A. (1993). Exploring chemistry with electronic structure methods. Gaussian, Inc.

Ghosh P., Adkins J., Affek H. P., Balta B., Guo W., Schauble E. A., Schrag D. and Eiler J. M. (2006) ^{13}C–^{18}O bonds in carbonate minerals: a new kind of paleothermometer. *Geochim. Cosmochim. Acta* **70**, 1439–1456.

Ghosh P., Eiler J., Campana S. E. and Feeney R. F. (2007) Calibration of the carbonate'clumped isotope' paleothermometer for otoliths. *Geochim. Cosmochim. Acta* **71**, 2736–2744.

Gilg H. A., Struck U., Vennemann T. and Boni M. (2003) Phosphoric acid fractionation factors for smithsonite and cerussite between 25 and 72 °C. *Geochim. Cosmochim. Acta* **67**, 4049–4055.

Hage W., Liedl K. R., Hallbrucker A. and Mayer E. (1998) Carbonic acid in the gas phase and its astrophysical relevance. *Science* **279**, 1332–1335.

Kerisit S., Parker S. C. and Harding J. H. (2003) Atomistic simulation of the dissociative adsorption of water on calcite surfaces. *J. Phys. Chem. B* **107**, 7676–7682.

Kim S.-T., Mucci A. and Taylor B. E. (2007) Phosphoric acid fractionation factors for calcite and aragonite between 25 and 75 °C: revisited. *Chem. Geol.* **246**, 135–146.

Kim S.-T. and O'Neil J. R. (1997) Equilibrium and nonequilibrium oxygen isotope effects in synthetic carbonates. *Geochim. Cosmochim. Acta* **61**, 3461–3475.

Land, L.S. (1980). The isotopic and trace element geochemistry of dolomite: the state of the art.In SEPM Special Publications. 28. 87-110.

Lasaga A. C. (1998) *Kinetic Theory in the Earth Science*. Princeton University Press.

Li W. J. and Meijer H. A. J. (1998) The use of electrolysis for accurate $\delta^{17}O$ and $\delta^{18}O$ isotope measurements in water. *Isot. Environ. Health Stud.* **34**, 349–369.

Loerting T., Tautermann C., Kroemer R. T., Kohl I., Hallbrucker A., Mayer E. and Liedl K. R. (2000) On the surprising kinetic stability of carbonic acid (H_2CO_3). *Angew. Chem. Int. Ed.* **39**, 892–894.

Mao Y. and Siders P. D. (1997) Molecular Hartree–Fock model of calcium carbonate. *J. Mol. Struct. Theochem.* **419**, 173–184.

McCrea J. M. (1950) The isotopic chemistry of carbonates and a paleo-temperature scale. *J. Chem. Phys.* **18**, 849–857.

Melander L. and Saunders J. W. H. (1987) *Reaction Rates of Isotopic Molecules*. John Wiley & Sons, Inc..

Miller M. F., Röckmann T. and Wright I. P. (2007) A general algorithm for the ^{17}O abundance correction to $^{13}C/^{12}C$ determinations from CO_2 isotopologue measurements, including CO_2 characterised by 'mass-independent' oxygen isotope distributions. *Geochim. Cosmochim. Acta* **71**, 3145–3161.

O'Neil J. R. (1986) Theoretical and experimental aspects of isotopic fractionation. *Rev. Mineral.* **16**, 1–40.

Ramirez J.-Z., Vargas R., Garza J. and Hay B. P. (2006) Performance of the effective core potentials of Ca, Hg, and Pb in complexes with ligands containing N and O donor atoms. *J. Chem. Theory Comput.* **2**, 1510–1519.

Ringnalda, M.N., Langlois, J.-M., Greeley, B.H., Russo, T.V., Muller, R.P., Marten, B., Won, Y., Donnelly, R.E., Pollard, J., Thomas, W., Miller, G.H., Goddard, W.A.I., Friesner, R.A. (2005). Jaguar, version 6.5. Schrodinger, LLC, New York, NY.

Rollion-Bard C., Mangin D. and Champenois M. (2007) Development and application of oxygen and carbon isotopic measurements of biogenic carbonates by ion microprobe. *Geostand. Geoanal. Res.* **31**, 39–50.

Rosenbaum J. and Sheppard S. M. F. (1986) An isotopic study of siderites, dolomites and ankerites at high temperatures. *Geochim. Cosmochim. Acta* **50**, 1147–1150.

Ruuska H., Hirva P. and Pakkanen T. A. (1999) Cluster models for calcite surfaces: ab initio quantum chemical studies. *J. Phys. Chem. B* **103**, 6734–6740.

Schauble E. A., Ghosh P. and Eiler J. M. (2006) Preferential formation of ^{13}C–^{18}O bonds in carbonate minerals, estimated using first-principles lattice dynamics. *Geochim. Cosmochim. Acta* **70**, 2510–2529.

Scott A. P. and Radom L. (1996) Harmonic vibrational frequencies: an evaluation of Hartree–Fock, Moeller–Plesset, Quadratic Configuration Interaction, Density Functional Theory, and semiempirical scale factors. *J. Phys. Chem.* **100**, 16502–16513.

Sharma S. K. and Sharma T. (1969a) Oxygen isotope fractionation factor between carbon dioxide and carbonate ion. *Int. J. Mass Spectrom. Ion Phys* **2**, 367–371.

Sharma S. K. and Sharma T. (1969b) Intramolecular kinetic isotope effect in the acid decomposition of carbonates. *Int. J. Mass Spectrom. Ion Phys.* **2**, 485–493.

Sharma T. and Clayton R. N. (1965) Measurement of $^{18}O/^{16}O$ ratios of total oxygen of carbonates. *Geochim. Cosmochim. Acta* **29**, 1347–1354.

Sharp Z. D. and Cerling T. E. (1996) A laser GC-IRMS technique for in situ stable isotope analyses of carbonates and phosphates. *Geochim. Cosmochim. Acta* **60**, 2909–2916.

Suito K., Namba J., Horikawa T., Taniguchi Y., Sakurai N., Kobayashi M., Onodera A., Shimomura O. and Kikegawa T. (2001) Phase relations of $CaCO_3$ at high pressure and high temperature. *Am. Mineral.* **86**, 997–1002.

Swart P. K., Burns S. J. and Leder J. J. (1991) Fractionation of the stable isotopes of oxygen and carbon in carbon dioxide during the reaction of calcite with phosphoric acid as a function of temperature and technique. *Chem. Geol.* **86**, 89–96.

Tossell J. A. (2006) H_2CO_3 and its oligomers: structures, stabilities, vibrational and NMR spectra, and acidities. *Inorg. Chem.* **45**, 5961–5970.

Urey H. C. (1947) Thermodynamic properties of isotopic substances. *J. Chem. Soc.*, 562–581.

Wang Z., Schauble E. A. and Eiler J. M. (2004) Equilibrium thermodynamics of multiply substituted isotopologues of molecular gases. *Geochim. Cosmochim. Acta* **68**, 4779–4797.

Associate editor: Juske Horita